

Functional Time Series Forecasting: Functional Singular Spectrum Analysis Approaches

Jordan Trinka

Department of Mathematical and Statistical Sciences,
Marquette University, USA

and

Hossein Haghbin*

Department of Statistics,
Persian Gulf University, Iran

and

Mehdi Maadooliat

Department of Mathematical and Statistical Sciences,
Marquette University, USA

Abstract

In this paper, we propose two nonparametric methods used in the forecasting of functional time-dependent data, namely functional singular spectrum analysis recurrent forecasting and vector forecasting. Both algorithms utilize the results of functional singular spectrum analysis and past observations in order to predict future data points where recurrent forecasting predicts one function at a time and the vector forecasting makes predictions using functional vectors. We compare our forecasting methods to a gold standard algorithm used in the prediction of functional, time-dependent data by way of simulation and real data and we find our techniques do better for periodic stochastic processes.

Keywords: Singular Spectrum Analysis, Functional Time Series, Hilbert Space, Forecasting

*Contributed equally as much as first author

1 Introduction

Functional data analysis (FDA) is a growing field of statistics that is showing promising results in analysis due to the fact that functional algorithms act on possibly more informative and smooth data. Often times statistical techniques that act on real-valued scalars or vectors are extended into the functional realm to handle such curved data. One example is principal component analysis (PCA) which was extended into functional PCA (FPCA) and multivariate FPCA so that dimension reduction may be performed on time-independent functional observations and many variants of these methods have been developed, see Ramsay and Silverman (2005), Jeng-Min et al. (2014), and Happ and Greven (2018) for more details. Another example of this concept can be seen in singular spectrum analysis (SSA) (Golyandina et al., 2001) which is a decomposition technique for time series. The SSA algorithm was extended into functional SSA (FSSA) in Haghbin et al. (2020a). They showed that the FSSA algorithm outperforms SSA and FPCA-based approaches in separating out sources of variation for smooth, time-dependent, functional data which is defined as a functional time series (FTS). In addition to SSA being extended to FSSA, the multivariate SSA (MSSA) approaches (Golyandina et al., 2015; Hassani and Mahmoudvand, 2013) have also been extended to the functional realm in Trinkka et al. (2020) where dimension reduction was performed on a multivariate FTS of intraday temperature curves and images of vegetation in a joint analysis giving more prominent results.

An important problem often confronted by researchers is prediction of stochastic processes. Golyandina et al. (2001) expanded the results of the SSA and MSSA algorithms to deliver a nonparametric forecasting method, called SSA recurrent forecasting, and Hassani

and Mahmoudvand (2013) developed the vector forecasting approach.¹ Since the aforementioned SSA techniques have seen success in forecasting time series data, one may seek expanding that to the functional world for forecasting FTS.

One of the first approaches to FTS forecasting is given in Hyndman and Ullah (2007) who found success in predicting mortality rates data. The method of Hyndman and Ullah (2007) has been extended so that more recent FTS observations play a larger role in forecasts (Hyndman and Shang, 2009). In addition, extensions have been made so that the method is robust in the presence of outliers (Shang, 2019; Beyaztas and Shang, 2019). The approach of Hyndman and Ullah (2007) has also inspired a functional extension to the ARMAX model González et al. (2018) allowing for estimation of moving average terms. In addition, the methodology of Hyndman and Ullah (2007) and its variants have seen success in applications other than just mortality rate data, see Shang (2013) and Wagner-Muns et al. (2018).

The approach of Hyndman and Ullah (2007) and its extensions consists of two steps. In the first step, they use FPCA, or its variants, to reduce the dimensionality of the functional data and project the curves onto the FPCA basis. In the second step, they perform forecasting of the basis coefficient using various techniques such as ARIMA. The details of the technique of Hyndman and Ullah (2007) are given in the supplementary material. One may argue the time-dependency is not considered in the first step of their algorithm. In this paper we develop two forecasting algorithms based on FSSA that can incorporate the time-dependency into the decomposition of FTS. Furthermore, the proposed algorithms do not need the stationary assumption.

In order to depict the idea of our approach and to show its utility, consider the following

¹See the Appendix for a brief review of SSA and its respective forecasting approaches.

motivating example involving a real dataset which is described in detail in Subsection 4.2. Here we consider a FTS of 365 curves where each function describes the square root of the number of calls, aggregated every six minutes, to a call center, in a day between January 1st, 1999 to December 31st, 1999 given in Figure 1.

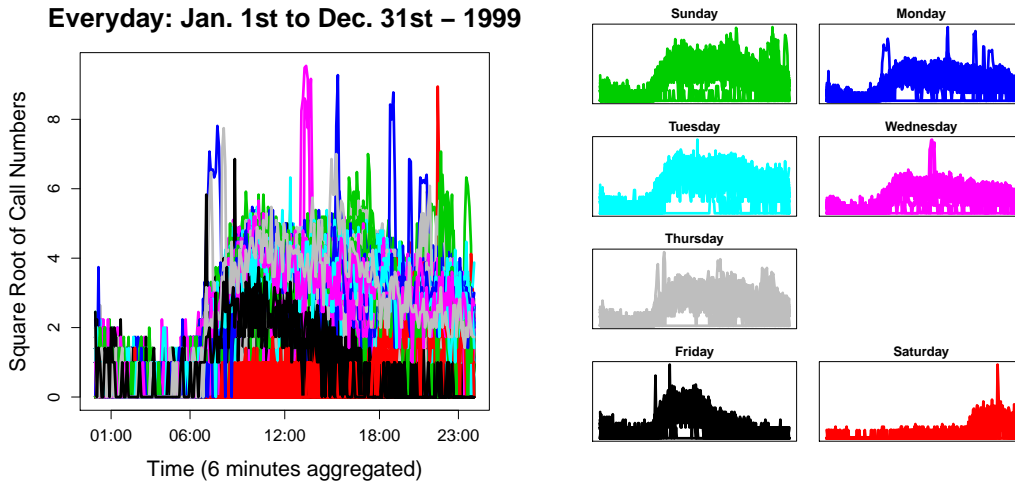


Figure 1: The square root of the number of calls to a call center

Researchers have analyzed this data several times using FPCA-based approaches, see Shen and Huang (2005), Huang et al. (2008), and Maadooliat et al. (2015) and the data has been analyzed in the FSSA approach of Haghbin et al. (2020a). Here we see that there exists a strong weekly periodicity in the data between workdays (Sunday through Thursday) and non-workdays (Friday and Saturday). We partition the $N = 365$ curves into a training set of size $M = 308$ (curves observed starting January 1, 1999 and ending November 4, 1999) and a testing set of the remaining 57 (curves observed starting November 5, 1999 and ending December 31, 1999) functions. We compare our proposed methodologies of FSSA

recurrent forecasting (R-forecasting) and FSSA vector forecasting (V-forecasting) to the approach of Hyndman and Ullah (2007) in a rolling forecast fashion to obtain Figure 2.

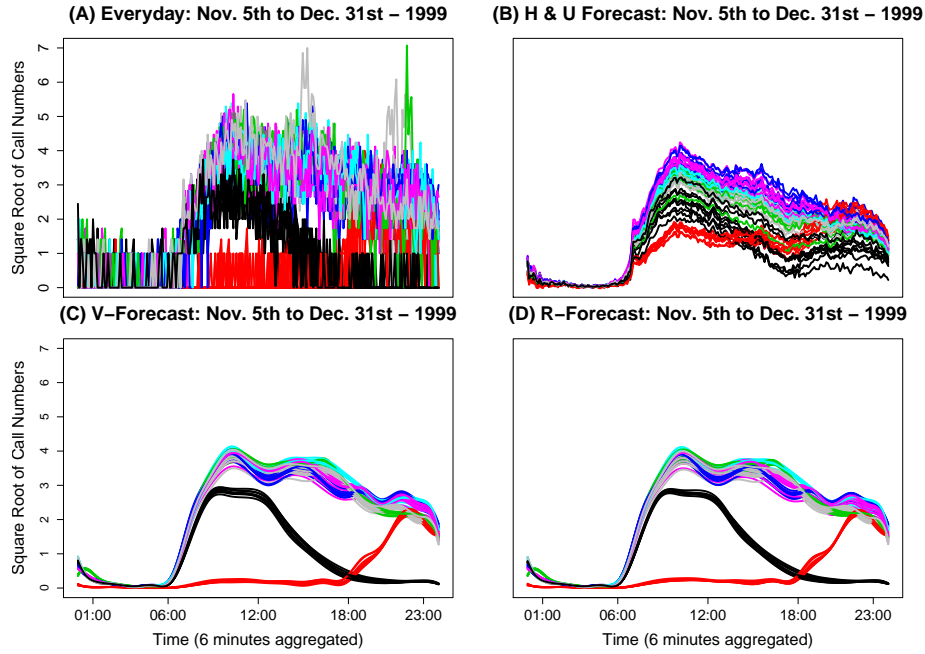


Figure 2: Plot (A): testing set; Plot (B): predictions using method of Hyndman and Ullah (2007); Plot (C): FSSA V-forecasting predictions; Plot (D): FSSA R-forecasting predictions.

We see that the popular method of Hyndman and Ullah (2007) struggles in prediction of the periodic call center data especially when trying to differentiate workdays from non-workdays, while our methods of FSSA R-forecasting and V-forecasting can capture this periodic behavior and reflect that in the prediction.

The rest of the manuscript is organized as follows. In Section 2, we review the method-

ology of FSSA through the decomposition stage and we theoretically derive the FSSA R-forecasting and V-forecasting algorithms. Then in Section 3 we give the recipes needed to implement the R-forecasting and V-forecasting approaches. Section 4 gives a simulation study and a real data study showing how our methods outperform a functional seasonal naive method and the popular technique of Hyndman and Ullah (2007) in forecasting periodic FTS. Finally, we end with a discussion on results in Section 5.

2 FSSA Forecasting

We begin with some notations leveraged in the FSSA decomposition routine. We consider $\mathbf{y}_N = (y_1, \dots, y_N)^\top$ as a FTS of length N such that each $y_i : [0, 1] \rightarrow \mathbb{R}$ belongs to $\mathbb{H} = \mathcal{L}^2([0, 1])$ where $\mathcal{L}^2([0, 1])$ is the space of square integrable real functions defined on the interval $[0, 1]$. For some x, y in the Hilbert space, \mathbb{H} , we have that the inner product equipped to \mathbb{H} is given by $\langle x, y \rangle_{\mathbb{H}} = \int_0^1 x(s) y(s) ds$. For a positive integer m , the space, \mathbb{H}^m , denotes the Cartesian product of m copies of \mathbb{H} ; such that any $\mathbf{x} \in \mathbb{H}^m$ has the form $\mathbf{x}(s) = (x_1(s_1), x_2(s_2), \dots, x_m(s_m))^\top$, where $x_i \in \mathbb{H}$, $\mathbf{s} = (s_1, s_2, \dots, s_m)$ and $s_i \in [0, 1]$. For some \mathbf{x}, \mathbf{y} in the Hilbert space, \mathbb{H}^m , we define the inner product as $\langle \mathbf{x}, \mathbf{y} \rangle_{\mathbb{H}^m} = \sum_{i=1}^m \langle x_i, y_i \rangle_{\mathbb{H}}$. We denote the norms by $\|\cdot\|_{\mathbb{H}}$ and $\|\cdot\|_{\mathbb{H}^m}$ in the spaces \mathbb{H} and \mathbb{H}^m respectively. Given $x, y \in \mathbb{H}$, then the tensor (outer) product of these two elements gives us the operator $x \otimes y : \mathbb{H} \rightarrow \mathbb{H}$ where for some $h \in \mathbb{H}$, we have $(x \otimes y)h = \langle x, h \rangle_{\mathbb{H}} y$.

For positive integers L and K , we denote $\mathbb{H}^{L \times K}$ as the linear space spanned by operators $\mathbf{Z} : \mathbb{R}^K \rightarrow \mathbb{H}^L$, specified by $[z_{i,j}]_{i=1, \dots, L}^{j=1, \dots, K}$ where

$$\mathbf{Z}\mathbf{a} = \begin{pmatrix} \sum_{j=1}^K a_j z_{1,j} \\ \vdots \\ \sum_{j=1}^K a_j z_{L,j} \end{pmatrix}, \quad z_{i,j} \in \mathbb{H}, \text{ and } \mathbf{a} = (a_1, \dots, a_K) \in \mathbb{R}^K.$$

We call an operator $\tilde{\mathbf{Z}} = [\tilde{z}_{i,j}] \in \mathbb{H}^{L \times K}$ Hankel if $\|\tilde{z}_{i,j} - g_s\|_{\mathbb{H}} = 0$ for some $g_s \in \mathbb{H}$, where $s = i + j$. The space of such Hankel operators will be denoted with $\mathbb{H}_H^{L \times K}$. For two given operators $\mathbf{Z}_1 = [z_{i,j}^{(1)}]_{i=1,\dots,L}^{j=1,\dots,K}$ and $\mathbf{Z}_2 = [z_{i,j}^{(2)}]_{i=1,\dots,L}^{j=1,\dots,K}$ in $\mathbb{H}^{L \times K}$, define

$$\langle \mathbf{Z}_1, \mathbf{Z}_2 \rangle_{\mathcal{F}} = \sum_{i=1}^L \sum_{j=1}^K \left\langle z_{i,j}^{(1)}, z_{i,j}^{(2)} \right\rangle_{\mathbb{H}}.$$

It follows immediately that $\langle \cdot, \cdot \rangle_{\mathcal{F}}$, defines an inner product on $\mathbb{H}^{L \times K}$. We will call it Frobenius inner product of two operators in $\mathbb{H}^{L \times K}$. The associated Frobenius norm is $\|\mathbf{Z}\|_{\mathcal{F}} = \sqrt{\langle \mathbf{Z}, \mathbf{Z} \rangle_{\mathcal{F}}}$. Now we jump into the FSSA procedure with the goal of extracting time-dependent modes of variation that can be used for forecasting.

2.1 FSSA Procedure

For an integer $1 < L < N/2$, let $K = N - L + 1$ and define a set of multivariate functional vectors in \mathbb{H}^L by

$$\mathbf{x}_j = (y_j, y_{j+1}, \dots, y_{j+L-1})^{\top}, \quad j = 1, \dots, K,$$

where \mathbf{x}_j 's denote the functional L -lagged vectors. We also have that L should be chosen to be a multiple of the periodicity present in the data (Hagbabin et al., 2020a). We now continue with the FSSA methodology.

Step 1. Embedding

In this first step we form the trajectory operator, $\mathcal{X} : \mathbb{R}^K \rightarrow \mathbb{H}^L$, which is defined by

$$\mathcal{X}\mathbf{a} = \sum_{j=1}^K a_j \mathbf{x}_j, \quad \mathbf{a} \in \mathbb{R}^K.$$

We see that the rank of \mathcal{X} is $0 < r \leq K$ and that the range of this operator includes all possible linear combinations of the functional L -lagged vectors. This step of embedding can also be view as applying the invertible operation $\mathcal{T} : \mathbb{H}^N \rightarrow \mathbb{H}_H^{L \times K}$ such that $\mathcal{T}(\mathbf{y}_N) = \mathcal{X}$.

Step 2. Decomposition

Since \mathcal{X} is of finite rank, then there exists orthonormal elements $\{\boldsymbol{\psi}_i\}_{i=1}^r$ from \mathbb{H}^L and orthonormal vectors $\{\mathbf{v}_i\}_{i=1}^r$ from \mathbb{R}^K such that

$$\mathcal{X}\mathbf{a} = \sum_{i=1}^r \sqrt{\lambda_i} \langle \mathbf{v}_i, \mathbf{a} \rangle_{\mathbb{R}^K} \boldsymbol{\psi}_i, \quad \text{for all } \mathbf{a} \in \mathbb{R}^K,$$

where λ_i 's are non-ascending positive scalars. We call the previous equation the fSVD of \mathcal{X} . We shall call $\sqrt{\lambda_i}$ as the i^{th} singular value, $\boldsymbol{\psi}_i$ as the i^{th} left singular function, and \mathbf{v}_i as the i^{th} right singular vector of the trajectory operator. Therefore we call the collection $\{\sqrt{\lambda_i}, \boldsymbol{\psi}_i, \mathbf{v}_i\}$ as the i^{th} eigentriple of \mathcal{X} . Now consider $\mathcal{X}_i : \mathbb{R}^K \rightarrow \mathbb{H}^L$ as the i^{th} rank one elementary operator defined by $\mathcal{X}_i = \sqrt{\lambda_i} \mathbf{v}_i \otimes \boldsymbol{\psi}_i$, which allows us to write

$$\mathcal{X} = \sum_{i=1}^r \mathcal{X}_i.$$

From here we move onto the grouping stage.

Step 3. Grouping

In grouping, we combine elementary operators together for reconstruction. For $m \leq r$, consider a disjoint partition $\{I_1, I_2, \dots, I_m\}$ of the set of indices $\{1, \dots, r\}$ and define $\mathbf{x}_{I_q} = \sum_{i \in I_q} \mathbf{x}_i$. This allows us to write

$$\mathbf{x} = \sum_{q=1}^m \mathbf{x}_{I_q}.$$

Note that we perform the grouping stage so that each of the m groups capture a different behavior of the original FTS such as mean, periodic, noise, etc. This can usually be done by using exploratory plots like scree plots, w -correlation plots, and paired-plots. We refer to Golyandina et al. (2001); Golyandina and Zhigljavsky (2013); Hassani and Mahmoudvand (2013); Haghbin et al. (2020a) for more information on these types of plots.

Step 4. Reconstruction

In reconstruction, we build a FTS that will be forecasted using our R-forecasting method and a linear operator that will be leveraged in V-forecasting. For each integer, q ($1 \leq q \leq m$), we would like to use $\mathcal{T}^{-1} : \mathbb{H}_H^{L \times K} \rightarrow \mathbb{H}^N$ to transform back each operator \mathbf{x}_{I_q} to an additive FTS, $\tilde{\mathbf{y}}_N^q \in \mathbb{H}^N$, where these elements describe a characteristic of the original FTS such as trend, periodicity, noise, etc. To do this, we first perform an orthogonal projection of each \mathbf{x}_{I_q} onto $\mathbb{H}_H^{L \times K}$, which is a closed subspace of $\mathbb{H}^{L \times K}$, with respect to the Frobenius norm. We denote the elements of \mathbf{x}_{I_q} and the corresponding orthogonal projection, $\tilde{\mathbf{x}}_{I_q} \in \mathbb{H}_H^{L \times K}$, with $[x_{i,j}^q]$ and $[\tilde{x}_{i,j}^q]$, respectively. Then, using the results of Haghbin et al. (2020a) we have that

$$\tilde{x}_{i,j}^q = \frac{1}{n_s} \sum_{(k,l):k+l=s} x_{k,l}^q,$$

where $s = i + j$ and n_s stands for the number of (l, k) pairs such that $l + k = s$. We denote this projection by $\mathbf{\Pi}_H : \mathbb{H}^{L \times K} \rightarrow \mathbb{H}_H^{L \times K}$ such that $\tilde{\mathcal{X}}_{I_q} = \mathbf{\Pi}_H \mathcal{X}_{I_q}$. From here, we find that $\tilde{\mathbf{y}}_N^q = \mathcal{T}^{-1} \tilde{\mathcal{X}}_{I_q}$. We let $J \subseteq \{1, \dots, m\}$, then we express our reconstructed signal as

$$\tilde{\mathbf{y}}_N = \sum_{q \in J} \tilde{\mathbf{y}}_N^q = (\tilde{y}_1, \dots, \tilde{y}_N)^\top.$$

In addition, we define

$$\mathcal{X}_J = \sum_{q \in J} \mathcal{X}_{I_q}$$

as an operator in $\mathbb{H}^{L \times K}$ whose range is linearly spanned by K elements of \mathbb{H}^L denoted by $\{(\mathbf{x}_J)_i\}_{i=1}^K$. This implies that for some $\mathbf{a} \in \mathbb{R}^K$, we have $\mathcal{X}_J(\mathbf{a}) = \sum_{i=1}^K a_i (\mathbf{x}_J)_i$. We also note that for forecasting purposes, reconstruction should be performed in such a way that only the deterministic nature of \mathbf{y}_N is captured in $\tilde{\mathbf{y}}_N$ and \mathcal{X}_J . This usually implies that the number of elements in J is strictly less than m . As a result, we have that the residual elements of the signal, \mathbf{y}_N , are captured in $\mathbf{y}_N - \tilde{\mathbf{y}}_N = \sum_{q \notin J} \tilde{\mathbf{y}}_N^q$ and we typically do not include these noisy modes of variation in SSA-based forecasts, see Golyandina et al. (2001); Golyandina and Zhigljavsky (2013); Golyandina et al. (2015); Hassani and Mahmoudvand (2013) for more information.

2.2 FSSA R-Forecasting and V-Forecasting

The following contains some notation that will be leveraged throughout the rest of this Section and Section 3. For each functional vector $\mathbf{x} \in \mathbb{H}^L$, denote by $\mathbf{x}^\nabla \in \mathbb{H}^{L-1}$ and

$\mathbf{x}^\Delta \in \mathbb{H}^{L-1}$ the functional vectors consisting of the first and the last (respectively) $L - 1$ components of the vector \mathbf{x} . Setting $k < r$, let us define $\mathcal{L} = \text{sp}\{\boldsymbol{\psi}_i\}_{i=1}^k$ and $\mathcal{L}^\nabla = \text{sp}\{\boldsymbol{\psi}_i^\nabla\}_{i=1}^k$. Moreover, let $\pi_i \in \mathbb{H}$ be the last component of the functional vector $\boldsymbol{\psi}_i$, $i = 1, \dots, k$. With this notation, we may continue into the theory of prediction.

Here, we offer an important theorem and corollary that will be leveraged in the FSSA R-forecasting and V-forecasting algorithms. All proofs of presented theory can be found in the supplementary materials.

Theorem 2.1. *Let $\mathcal{H} := \{(\mathbf{0}, \dots, \mathbf{0}, x)^\top \in \mathbb{H}^L | x \in \mathbb{H}\}$ and define the operator $\boldsymbol{\mathcal{V}} : \mathbb{H} \rightarrow \mathbb{H}$ such that $\boldsymbol{\mathcal{V}} := \sum_{n=1}^k \pi_n \otimes \pi_n$. If $\mathcal{H} \cap \mathcal{L} = \emptyset$, then we have that*

$$\|\boldsymbol{\mathcal{V}}\| = \sup_{\|x\|_{\mathbb{H}}=1} \|\boldsymbol{\mathcal{V}}(x)\|_{\mathbb{H}} < 1$$

where $\|\cdot\|$ is the operator norm.

Corollary 2.1. *Given that the conditions of Theorem 2.1 are met, we have that $\sum_{l=0}^{\infty} \boldsymbol{\mathcal{V}}^l$ is a convergent Neumann series and that $(\boldsymbol{\mathcal{I}} - \boldsymbol{\mathcal{V}})^{-1}$ exists. Furthermore, we obtain the equality*

$$(\boldsymbol{\mathcal{I}} - \boldsymbol{\mathcal{V}})^{-1} = \sum_{l=0}^{\infty} \boldsymbol{\mathcal{V}}^l$$

where $\boldsymbol{\mathcal{I}} : \mathbb{H} \rightarrow \mathbb{H}$ is the identity operator.

The primary assumption seen in Theorem 2.1 is that for some $\mathbf{z} \in \mathcal{H}$, we must have $\mathbf{z} \notin \mathcal{L}$ which is satisfied by choosing $k < r$. Now we define $\mathbf{g}_{N+M} = (g_1, \dots, g_N, g_{N+1}, \dots, g_{N+M})^\top \in \mathbb{H}^{N+M}$ as a FTS of length $N+M$ where we will determine the elements using our forecasting algorithms.

R-Forecasting

The SSA recurrent forecasting approach of Golyandina et al. (2001) leverages the fact that the next forecasted value of a time series can be expressed as a linear combination of the previous $L - 1$ scalar observations where the coefficients, a_j 's, can be viewed as weights as seen in (A1). When we migrate to the functional realm, we move towards linear combinations of functions where the coefficient scalar weights are replaced with operators that perform the weighting. With this in mind, we now give the following theorem which provides the FSSA R-forecasting algorithm.

Theorem 2.2. *Let $\mathcal{H} \cap \mathcal{L} = \emptyset$. Then we have that the entries of \mathbf{g}_{N+M} are given by*

$$g_i = \begin{cases} \tilde{y}_i & i = 1, \dots, N \\ \sum_{j=1}^{L-1} \mathcal{A}_j g_{i+j-L} & i = N+1, \dots, N+M \end{cases} \quad (1)$$

where $\mathcal{A}_j : \mathbb{H} \rightarrow \mathbb{H}$ is an operator defined by $\mathcal{A}_j = \sum_{n=1}^k \psi_{j,n} \otimes (\mathcal{I} - \mathcal{V})^{-1} \pi_n$ and $\psi_{j,n} \in \mathbb{H}$ is the j^{th} component of the n^{th} left singular function.

V-Forecasting

The R-forecasting can be extended into an algorithm that allows us to perform prediction using functional L -lagged vectors known as V-forecasting. We first define the operator, $\mathcal{P}^\nabla : \mathbb{R}^k \rightarrow \mathbb{H}^{L-1}$ such that for some $\mathbf{a} \in \mathbb{R}^k$, we have

$$\mathcal{P}^\nabla(\mathbf{a}) = \sum_{n=1}^k a_n \psi_n^\nabla.$$

We also define the adjoint, $(\mathcal{P}^\nabla)^* : \mathbb{H}^{L-1} \rightarrow \mathbb{R}^k$ such that for some $\mathbf{v} \in \mathbb{H}^{L-1}$, we have

$$(\mathcal{P}^\nabla)^*(\mathbf{v}) = \begin{bmatrix} \langle \mathbf{v}, \psi_1^\nabla \rangle_{\mathbb{H}^{L-1}} \\ \vdots \\ \langle \mathbf{v}, \psi_k^\nabla \rangle_{\mathbb{H}^{L-1}} \end{bmatrix}.$$

Using these definitions, we now give the following theorem which provides the FSSA V-forecasting algorithm.

Theorem 2.3. *Define the orthogonal projection onto \mathcal{L}^∇ as $\Pi : \mathbb{H}^{L-1} \rightarrow \mathbb{H}^{L-1}$ such that for some $\mathbf{v} \in \mathbb{H}^{L-1}$, we have*

$$\Pi(\mathbf{v}) := \mathcal{P}^\nabla ((\mathcal{P}^\nabla)^* \mathcal{P}^\nabla)^{-1} (\mathcal{P}^\nabla)^*(\mathbf{v}).$$

Now let $\mathcal{H} \cap \mathcal{L} = \emptyset$, and define the operator $\mathcal{Q} : \mathcal{L} \rightarrow \mathbb{H}^L$ such that for, some $\mathbf{x} \in \mathcal{L}$, we have

$$\mathcal{Q}(\mathbf{x}) = \begin{pmatrix} \Pi(\mathbf{x}^\Delta) \\ \sum_{j=1}^{L-1} \mathcal{A}_j(\Pi(\mathbf{x}^\Delta))_j \end{pmatrix} = \begin{pmatrix} \Pi(\mathbf{x}^\Delta) \\ \sum_{j=1}^{L-1} \mathcal{A}_j(\mathbf{x}^\Delta)_j \end{pmatrix}.$$

We construct the operator $\mathbf{Z}_J \in \mathbb{H}^{L \times (K+M)}$ whose range is linearly spanned by $K + M$ elements of \mathbb{H}^L , denoted with $\{(\mathbf{z}_J)_i\}_{i=1}^{K+M}$, such that for some $\mathbf{a} \in \mathbb{R}^{K+M}$, we have $\mathbf{Z}_J(\mathbf{a}) = \sum_{i=1}^{K+M} a_i (\mathbf{z}_J)_i$. We have that each $(\mathbf{z}_J)_i$ is given by

$$(\mathbf{z}_J)_i = \begin{cases} (\mathbf{x}_J)_i & i = 1, \dots, K \\ \mathcal{Q}(\mathbf{z}_J)_{i-1} & i = K + 1, \dots, K + M \end{cases} \quad (2)$$

just like in (A2) where each $(\mathbf{x}_J)_i$ was found in the reconstruction stage of FSSA from earlier in this section. We have that if we perform the Hankelization process on \mathbf{Z}_J to form $\tilde{\mathbf{Z}}_J \in \mathbb{H}_H^{L \times (K+M)}$, we may then extract the FTS, \mathbf{g}_{N+M} .

From here, we continue on with computer implementation of our algorithms.

3 Implementation Strategy

We start with some notation that will be leveraged in the implementation of the R-forecasting and V-forecasting algorithms. We assume that $\{\nu_i\}_{i=1}^d$ is a linearly independent basis for \mathbb{H}_d , which is a d -dimensional subspace of \mathbb{H} , such that for some $f \in \mathbb{H}_d$ there exists a unique vector of coefficients, $\mathbf{c}_f \in \mathbb{R}^d$, where

$$f = \sum_{i=1}^d (\mathbf{c}_f)_i \nu_i.$$

Let $f \in \mathbb{H}_d$ and define $\mathbf{G} = [\langle \nu_i, \nu_j \rangle_{\mathbb{H}}]_{i,j=1}^d$ to be the $d \times d$ Gram matrix then we find that, $\mathbf{G}\mathbf{c}_f = (\langle \nu_1, f \rangle_{\mathbb{H}}, \dots, \langle \nu_d, f \rangle_{\mathbb{H}})^\top \in \mathbb{R}^d$. From hereafter, we consider all discussed operators whose domain or range are infinite dimensional Hilbert spaces to operate on or map to the corresponding d -dimensional subspace. Since the FSSA R-forecasting and V-forecasting algorithms are both dependent on $(\mathcal{I} - \mathcal{V})^{-1} : \mathbb{H}_d \rightarrow \mathbb{H}_d$, we explore one particular implementation of this quantity in the following lemma that will be leveraged in the recipes for R-forecasting and V-forecasting.

Lemma 3.1. *We define the $d \times k$ matrix, $\mathbf{D} = [\langle \nu_i, \pi_n \rangle]_{i=1, \dots, d}^{n=1, \dots, k}$, which allows us to write*

$$[\langle (\mathcal{I} - \mathcal{V})^{-1}(\pi_n), \nu_i \rangle_{\mathbb{H}}]_{i=1, \dots, d}^{n=1, \dots, k} = \left(\sum_{l=0}^{\infty} (\mathbf{D}\mathbf{D}^\top)^l \right) \mathbf{D}.$$

Recall that since $\|\mathcal{V}\| < 1$, the real-valued sequence, $(\|\mathcal{V}^l\|)_{l \in \mathbb{N}}$, converges to zero monotonically. As a result, we truncate $\sum_{l=0}^{\infty} (\mathbf{D}\mathbf{D}^\top)^l$ when $\|(\mathbf{D}\mathbf{D}^\top)^l\|_F \approx 0$ for some $l \in \mathbb{N}$ where $\|\cdot\|_F$ denotes the Frobenius norm of a matrix.

R-Forecasting

We now give the recipe for the implementation of the FSSA R-forecasting algorithm. As according to (1), our goal is to find the matrix that corresponds with each $\mathcal{A}_j : \mathbb{H}_d \rightarrow \mathbb{H}_d$ for $j = 1, \dots, L-1$. Leveraging ideas from Balazs (2009) we find the implementation of R-forecasting in the following theorem.

Theorem 3.1. *Denote by $\mathbf{A}_j \in \mathbb{R}^{d \times d}$, the matrix that corresponds with \mathcal{A}_j and let $\mathbf{E}_j = [\langle \nu_i, \psi_{j,n} \rangle_{\mathbb{H}}]_{i=1, \dots, d}^{n=1, \dots, k}$ be a $d \times k$ matrix for $j = 1, \dots, L-1$, then we obtain the following*

$$\mathbf{A}_j = \left(\sum_{l=0}^{\infty} (\mathbf{D}\mathbf{D}^\top)^l \right) \mathbf{D}\mathbf{E}_j^\top.$$

Now, if $\mathcal{H} \cap \mathcal{L} = \emptyset$, we find the coefficients of the left-hand side of (1) as

$$\mathbf{G}\mathbf{c}_{g_i} = \begin{cases} \mathbf{G}\mathbf{c}_{\tilde{y}_i} & i = 1, \dots, N \\ \sum_{j=1}^{L-1} \mathbf{A}_j \mathbf{G}\mathbf{c}_{g_{i+j-L}} & i = N+1, \dots, N+M \end{cases} \quad (3)$$

V-Forecasting

In order to obtain the recipes for the FSSA V-forecast, we first leverage theory developed in Haghighi et al. (2020a). For some positive integer, L , we define \mathbb{H}_d^L to be the space created from the Cartesian product of L copies of \mathbb{H}_d . Now we define the quotient-remainder sequence

$$j = (q_j - 1)L + r_j, \quad 1 \leq q_j \leq d, \quad 1 \leq r_j \leq L$$

and from here we define the collection of linearly independent elements $\{\phi_j\}_{j=1}^{Ld}$ where $\phi_j \in \mathbb{H}_d^L$ is the zero function in all coordinates except for the r_j^{th} which is ν_{q_j} . We find that the basis, $\{\phi_j\}_{j=1}^{Ld}$, linearly spans \mathbb{H}_d^L . This implies that for any $\mathbf{f} \in \mathbb{H}_d^L$, there exists a unique vector, $\mathbf{c}_f \in \mathbb{R}^{Ld}$, such that

$$\mathbf{f} = \sum_{i=1}^{Ld} (\mathbf{c}_f)_i \phi_i.$$

From here, we define the $Ld \times Ld$ Gram matrix, $\mathbf{H} = [\langle \phi_i, \phi_j \rangle_{\mathbb{H}^L}]_{i,j=1}^{Ld}$. Now, we define the new, truncated quotient-remainder sequence as

$$i = (q_i - 1)(L - 1) + r_i, \quad 1 \leq q_i \leq d, \quad 1 \leq r_i \leq L - 1.$$

This allows us to define $\{\phi_i^\nabla\}_{i=1}^{(L-1)d}$ where $\phi_i^\nabla \in \mathbb{H}_d^{L-1}$ is zero in all coordinates except for the r_i^{th} which is ν_{q_i} . Similar to the non-truncated case we find that for any $\mathbf{f}^\nabla \in \mathbb{H}_d^{L-1}$, there exists a unique vector $(\mathbf{c}_{f^\nabla}) \in \mathbb{R}^{(L-1)d}$, such that

$$\mathbf{f}^\nabla = \sum_{i=1}^{(L-1)d} (\mathbf{c}_{f^\nabla})_i \phi_i^\nabla.$$

We also find that any $\mathbf{f}^\Delta \in \mathbb{H}_d^{L-1}$ may be expanded out in the same manner as seen in the previous equation, using the same basis of $\{\phi_i^\nabla\}_{i=1}^{(L-1)d}$. We define the $(L - 1)d \times (L - 1)d$ Gram matrix, $\mathbf{H}^\nabla = [\langle \phi_i^\nabla, \phi_j^\nabla \rangle_{\mathbb{H}^{L-1}}]_{i,j=1}^{(L-1)d}$, and now we must find the corresponding matrix of $\mathbf{\Pi} : \mathbb{H}_d^{L-1} \rightarrow \mathbb{H}_d^{L-1}$. We again use ideas from Balazs (2009) in the development of the following theorem which gives the implementation of V-forecasting.

Theorem 3.2. *Denote by $\mathbf{P} \in \mathbb{R}^{(L-1)d \times (L-1)d}$ as the matrix that corresponds with $\mathbf{\Pi}$ and define $\mathbf{F} = [\langle \phi_i^\nabla, \psi_n^\nabla \rangle_{\mathbb{H}^{L-1}}]_{i=1, \dots, (L-1)d}^{n=1, \dots, k}$, then we obtain the following*

$$\mathbf{P} = \mathbf{F}\mathbf{F}^\top + \mathbf{F}\mathbf{D}^\top \sum_{l=0}^{\infty} (\mathbf{D}\mathbf{D}^\top)^l \mathbf{D}\mathbf{F}^\top$$

Let $\mathcal{H} \cap \mathcal{L} = \emptyset$ and define $\mathbf{Q} \in \mathbb{R}^{Ld \times Ld}$ to be the matrix that corresponds with \mathcal{Q} , then we find for some $\mathbf{x} \in \mathcal{L}$

$$\mathbf{Q}(\mathbf{H}\mathbf{c}_{\mathbf{x}}) = \begin{pmatrix} \mathbf{P}(\mathbf{H}^\nabla \mathbf{c}_{\mathbf{x}^\Delta}) \\ \sum_{j=1}^{L-1} \mathbf{A}_j (\mathbf{P}(\mathbf{H}^\nabla \mathbf{c}_{\mathbf{x}^\Delta}))_j \end{pmatrix} = \begin{pmatrix} \mathbf{P}(\mathbf{H}^\nabla \mathbf{c}_{\mathbf{x}^\Delta}) \\ \sum_{j=1}^{L-1} \mathbf{A}_j (\mathbf{H}^\nabla \mathbf{c}_{\mathbf{x}^\Delta})_j \end{pmatrix}.$$

From here, we define the $Ld \times (K + M)$ matrix that corresponds with \mathbf{Z}_J as

$$\mathbf{Z}_J = \left[\mathbf{H}\mathbf{c}_{(\mathbf{z}_J)_1}, \dots, \mathbf{H}\mathbf{c}_{(\mathbf{z}_J)_{K+M}} \right] \text{ where}$$

$$\mathbf{H}\mathbf{c}_{(\mathbf{z}_J)_i} = \begin{cases} \mathbf{H}\mathbf{c}_{(\mathbf{x}_J)_i} & i = 1, \dots, K \\ \mathbf{Q}(\mathbf{H}\mathbf{c}_{(\mathbf{z}_J)_{i-1}}) & i = K + 1, \dots, K + M \end{cases} \quad (4)$$

just like in (2). If we Hankelize \mathbf{Z}_J , we may extract the coefficients of each element in \mathbf{g}_{N+M} .

4 Numerical Studies

In this section, we offer a simulation study and a real data study that both showcase the advantage of our novel methods in forecasting periodic FTS. In the simulation study, we compare our approaches with a functional seasonal naive method and we also compare to the popular FTS forecasting technique of Hyndman and Ullah (2007), which we call the competing method. We incorporate either seasonality, increasing trend, or both in various simulation setups. We further illustrate the superior performance in forecasting of a periodic FTS with a real data study where we compare our techniques with the

competing method when the optimal parameters are selected for each algorithm applied to highly periodic call center data, moderately periodic remote sensing data, and mortality rate data that has no periodic components. We note that when we state that we are using k eigentriples in a forecasts, that means we use k left singular functions in the prediction.

4.1 Simulation Study

For the simulation study, we use a setup that is similar to that seen in Haghbin et al. (2020a) and Trinkka et al. (2020) where varying cases will generate FTS that have only periodicity or only trend or both. This particular setup utilizes FTS of lengths $N = 100, 200$ that are observed on $n = 100$ fixed, equidistant discrete points on the unit interval from the following model:

$$Y_t(s_i) = m_t(s_i) + X_t(s_i), \quad s_i \in [0, 1], i = 1, \dots, n, \text{ and } t = 1, \dots, N.$$

We use a B-spline basis with 15 degrees of freedom to smooth the discrete samplings of functional curves. We have that $m_t(s)$ is the true underlying signal to be extracted and predicted where

$$m_t(s) = \kappa t + e^{s^2} \cos(2\pi\omega t) + \cos(4\pi s) \sin(2\pi\omega t)$$

and we allow the trend coefficient, κ , to take on values of 0 and 0.02 while the frequency, ω , takes on the values of 0 or 0.20 in varying setups. We also have that $X_t(s)$ is a stochastic term that follows a functional autoregressive model of order 1, FAR(1), defined by

$$X_t(s) = \Psi X_{t-1}(s) + \epsilon_t(s),$$

where Ψ is an integral operator with a parabolic kernel as follows

$$\psi(s, u) = \gamma_0 \left(2 - (2s - 1)^2 - (2u - 1)^2 \right).$$

We choose γ_0 such that the Hilbert-Schmidt norm defined by

$$\|\Psi\|_{\mathcal{S}}^2 = \int_0^1 \int_0^1 |\psi(s, u)|^2 ds du,$$

takes on values of 0.25, 0.60, 0.90, and 0.95. We also consider the terms $\epsilon_t(s)$ to be independent trajectories of standard Brownian motion over $[0, 1]$. We will be comparing our recurrent forecast (RFSSA) to our vector forecast (VFSSA) with varying lags, L , of 10 and 20 and we compare both of these methods to a functional seasonal naive method (SNM) and the competing method (H & U). We choose the cases for the lag parameter in accordance with SSA literature where L is often chosen to be a multiple of the periodicity in the data, see Golyandina et al. (2001), Haghbin et al. (2020a), and Trinkka et al. (2020). In addition, we choose the optimal number of eigentriples to perform reconstructions and forecasts in FSSA-based models for each combination of κ and ω (two when $\kappa = 0$, $\omega = 0.20$, three when $\kappa = 0.02$, $\omega = 0.20$, and one when $\kappa = 0.02$, $\omega = 0$). We have that the maximum number of left singular functions chosen in the FSSA-based predictions is three (when $\kappa = 0.02$ and $\omega = 0.20$) and due to this, we choose three functional principal components to perform all forecasts in the method of Hyndman and Ullah (2007) for the simulations.

We expect that since our methods incorporate periodicity into the left singular functions that are used in the forecast, our techniques will perform better than the competing approach in predicting periodic true signals. To perform the comparison, we leverage a rolling forecast where the size of our training set, M , takes on values of 60 and 80. Since the implementation of the method of Hyndman and Ullah (2007), found in the R package

ftsa (Hyndman and Shang, 2020), takes in FTS inputs that are built from the **rainbow** R package Shang and Hyndman (2019) which does not allow the user to select the basis elements for fitting FTS observations, we leverage a measure of prediction error that is based off of function evaluations. We denote the forecast of the t^{th} function evaluated at $s_i \in [0, 1]$ with $\hat{Y}_t(s_i)$, which allows us to define the root mean square error of

$$RMSE = \sqrt{\frac{1}{(N-M) \times n} \sum_{t=1}^{N-M} \sum_{i=1}^n \left(\hat{Y}_{t+M}(s_i) - m_{t+M}(s_i) \right)^2}.$$

From here, we replicate the result of each simulation setup combination 100 times and report the mean of the RMSE's in Figure 3.

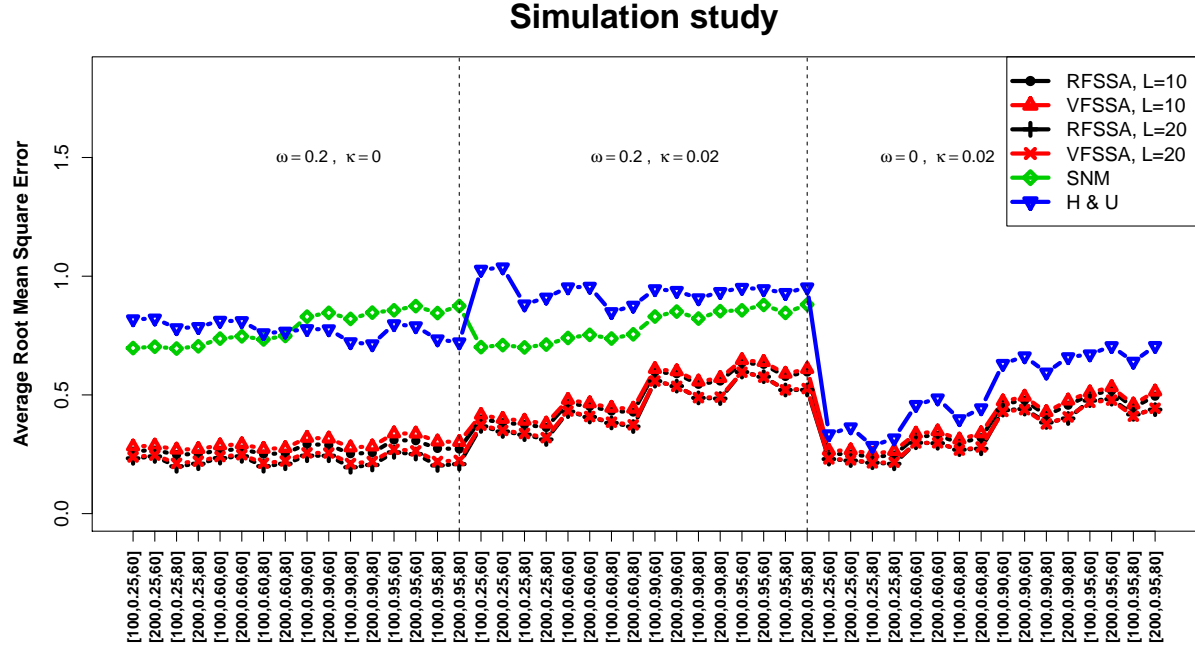


Figure 3: Simulation study where horizontal axis entries have form of $[N, \|\Psi\|_{\mathcal{S}}^2, M]$.

We find that our novel approaches consistently outperform SNM and the competing methodology for all setups. These results further illustrate the superior performance of our novel methodologies in predicting the true underlying signal when periodicity is present in the data and how our methods are still competitive for data that have no oscillatory elements. For a visuanimation that displays a sample of the simulation setups and some of the graphical results, see the supplementary material.

As an additional note on this simulation study, we do not vary standard deviation since it is obvious SNM will be better for smaller errors and worse for larger errors. In addition, we note that principal components that account for small variation in the data can still play a big role in improving predictions in principal component regression, see Jolliffe (1982) and references therein. This implies that we may need to use more than three functional principal components when applying the method of Hyndman and Ullah (2007) in our simulation study. In regards to the process of dimension reduction, the fact that our methodologies outperform the method of Hyndman and Ullah (2007) with such few eigentriples used in the forecasts is a bonus of our FSSA-based approaches since we wish to perform predictions using fewer elements. Still it would be interesting to compare our proposed methodologies to that of Hyndman and Ullah (2007) when the optimal model is chosen for each routine. In the following real data study, for highly periodic FTS, we showcase that our methodologies still outperform the FPCA-based technique of Hyndman and Ullah (2007) even when the optimal number of functional principal components are chosen for the competing algorithm.

4.2 Real Data Study

From the simulation study, we find that our methodologies are the superior choice in forecasting simulated periodic FTS as compared to the competing method when the optimal number of eigentriples are chosen for FSSA-based algorithms and three functional principal components are chosen for forecasts in the method of Hyndman and Ullah (2007). In the spirit of further showcasing this phenomenon continues when the optimal number of functional principal components are chosen to perform predictions in the method of Hyndman and Ullah (2007), we first introduce three real FTS each with varying levels of periodicity and trend being present. The first FTS is the call center data analyzed in Section 1 and we show this data again in plot (A) of Figure 4. The next is NDVI remote sensing data where NDVI images can be used to remotely track changes in vegetation (Panuju and Trisasongko, 2012; Tuck et al., 2014; Lambin, 1999). NDVI values closer to zero are indicative of less vegetation being present in a part of an image while values closer to one are indicative of more vegetation being present. From NDVI images taken of Jambi, Indonesia between February 18, 2000 and July 28, 2019 in 16 day increments, we estimate 448 densities of NDVI values using Silverman’s rule of thumb (Silverman, 1986), which can be seen in plot (B). We also note that an example of an NDVI image and associated density can be found in the supplementary material. The final is a dataset of 97 functions representative of mortality rate data of Swedish males between ages 0 and 100 for years 1899 to 1995 seen in plot (C) (University of California at Berkely (USA) and Max Planck Institute for Demographic Research, 2020).

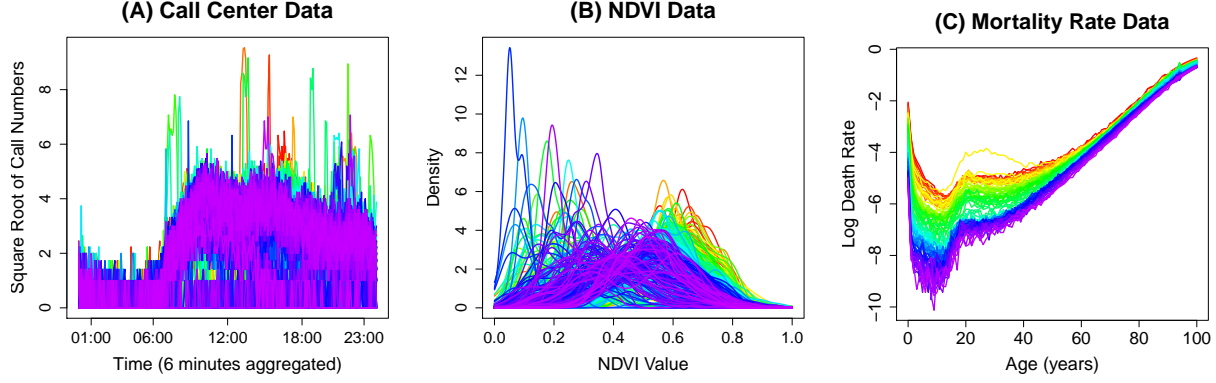


Figure 4: Plot (A): call center data, Plot (B): NDVI densities, Plot: (C) Swedish mortality rate data. warm colors, such as red and yellow, are indicative of curves observed on earlier dates while cool colors, such as blue and purple, are indicative of curves observed on later dates . Figures generated using the **rainbow** package (Shang and Hyndman, 2019).

As noted in Figure 4, warmer colors indicate observations occurring on earlier dates while cooler colors are indicative of earlier dates in each data set respectively and we can infer from these plots existence of periodic and trend behaviors present in each data set. Plot (A) in Figure 4 clearly shows periodic behavior with no trend as all warmer colors are covered with cooler colors. This strong, weekly periodicity for the call center data is also uncovered in Haghbin et al. (2020a) and a summary of the results are given in the supplementary materials. Plot (B) shows a slight decrease in NDVI values over time since densities observed in earlier dates (warmer colors) cluster around NDVI values of 0.6 while densities observed in later dates (cooler colors) cluster around 0.5. The existence of such a decreasing trend and an annual periodic behavior are confirmed by the work of Haghbin et al. (2020a) and we offer an outline of these results in the supplement. Finally, we see a strong decreasing trend with no periodicity in the mortality rate data of plot (C). Due to

the fact that our novel methods appear to perform best when a FTS is periodic as shown in Subsection 4.1, we expect our novel methods to perform better than the competing method for the highly periodic call center data, we expect a close competition for the NDVI densities, and we expect the competing method to perform best for the mortality rate data that lacks any periodicity.

As according to the work of Haghbin et al. (2020a), for the FSSA-based prediction algorithms applied to call center data, we select $L = 28$ and the first seven eigentriples to construct our deterministic FTS in reconstruction and to perform the forecast. Also according to Haghbin et al. (2020a), for the FSSA-based algorithms applied to NDVI data, we select $L = 45$ and the first four eigentriples to build the FTS and perform the forecast. Since there are no periodic elements present in the mortality rate data, we cannot use the standard rule of leveraging a lag that is a multiple of the periodicity in the FTS for the FSSA-based algorithms. In addition, we must select the best number of eigentriples to reconstruct the deterministic signal and to do the prediction given some lag L for the mortality rate data. We also must select the optimal number of functional principal components to use in the forecasts while applying the method of Hyndman and Ullah (2007) to each of the three data sets. To achieve these goals, we look towards cross-validation via a rolling forecast. We first define prediction root mean square error by

$$prRMSE = \sqrt{\frac{1}{(N - M) \times n} \sum_{t=1}^{N-M} \sum_{i=1}^n \left(\hat{Y}_{t+M}(s_i) - Y_{t+M}(s_i) \right)^2} \quad (5)$$

where \hat{Y}_{t+M} is the prediction of observation Y_{t+M} , s_i is a point in the domain, n are the number of sampling points, N is the length of the FTS, and M is the training set size. We perform rolling forecasts with training set sizes of 308, 403, and 50 for the call center, NDVI,

and mortality data respectively (giving us testing set sizes of 57, 45, and 47 respectively), and we estimate $prRMSE$ as according to (5) for varying choices of parameters. We find that a lag of 24 and using the first eigentriple to perform reconstruction and forecasting in the FSSA-based algorithms applied to the mortality rate data minimize (5) for that data set. In terms of choosing the optimal number of functional principal components to perform the forecast in the method of Hyndman and Ullah (2007), we find choosing the first 33 functional principal components, the first eight functional principal components, and the first three functional principal components for the call center, NDVI, and mortality rate data respectively minimize (5). We report the prediction root mean square errors for each optimal model in Table 1.

Methodology	Call Center	NDVI	Mortality
V-Forecasting	0.567	0.824	0.227
R-Forecasting	0.569	0.827	0.236
Method of Hyndman and Ullah (2007)	0.855	0.818	0.143

Table 1: $prRMSE$'s of R-forecasting, V-forecasting, and the competing method of Hyndman and Ullah (2007) for various datasets

As seen in Table 1, our novel methodologies outperform for the highly periodic call center data. The three methods are comparable for the NDVI data which has a mixture of trend and periodic components. Finally, we see that the competing method does in fact perform better for the mortality rate data which contains no periodic components and only a decreasing trend.

5 Discussion

In this work, we developed efficient nonparametric FTS forecasting techniques that include periodicity into the basis elements. We compared our approaches with the competing method of Hyndman and Ullah (2007) and found our techniques are superior in forecasting periodic FTS since the FSSA routine captures time-dependency in the basis elements. As a result researchers can use our methodologies in order to obtain accurate and informative predictions of periodic stochastic processes.

References

- Balazs, P. (2009). Matrix representation of bounded linear operators by bessel sequences, frames and riesz sequence.
- Beyaztas, U. and Shang, H. L. (2019). Forecasting functional time series using weighted likelihood methodology. *Journal of Statistical Computation and Simulation*, 89(16):3046–3060.
- Golyandina, N., Korobeynikov, A., Shlemov, A., and Usevich, K. (2015). Multivariate and 2d extensions of singular spectrum analysis with the rssa package. *Journal of Statistical Software, Articles*, 67(2):1–78.
- Golyandina, N., Nekrutkin, V., and Zhigljavsky, A. A. (2001). *Analysis of time series structure: SSA and related techniques*. Chapman and Hall/CRC.
- Golyandina, N. and Zhigljavsky, A. (2013). *Singular spectrum analysis for time series*. Springer Science & Business Media.

- González, J. P., Muñoz San Roque, A. M. S., and Pérez, E. A. (2018). Forecasting functional time series with a new hilbertian armax model: Application to electricity price forecasting. *IEEE Transactions on Power Systems*, 33(1):545–556.
- Haghibin, H., Morteza Najibi, S., Mahmoudvand, R., Trink, J., and Maadooliat, M. (accepted 2020a). Functional Singular Spectrum Analysis. *Stat.* Retrieved from <https://arxiv.org/abs/1906.05232>.
- Haghibin, H., Morteza Najibi, S., Mahmoudvand, R., Trink, J., and Maadooliat, M. (accepted 2020b). Functional Singular Spectrum Analysis Supplementary Material. *Stat.* Retrieved from <https://arxiv.org/abs/1906.05232>.
- Happ, C. and Greven, S. (2018). Multivariate functional principal component analysis for data observed on different (dimensional) domains. *Journal of the American Statistical Association*, 113(522):649 – 659.
- Hassani, H. and Mahmoudvand, R. (2013). Multivariate singular spectrum analysis: A general view and new vector forecasting approach. *International Journal of Energy and Statistics*, 01(01):55–83.
- Huang, J. Z., Shen, H., Buja, A., et al. (2008). Functional principal components analysis via penalized rank one approximation. *Electronic Journal of Statistics*, 2:678–695.
- Hyndman, R. and Shang, H. L. (2009). Functional time series forecasting. *Journal of the Korean Statistical Society*, 38:199–211.
- Hyndman, R. and Shang, H. L. (2020). *ftsa: Functional Time Series Analysis*. R package version 5.9.0.

- Hyndman, R. and Ullah, S. (2007). Robust forecasting of mortality and fertility rates: A functional data approach. *Computational Statistics & Data Analysis*, 51:4942–4956.
- Jeng-Min, C., Yu-Ting, C., and Ya-Fang, Y. (2014). Multivariate functional principal component analysis: A normalization approach. *Statistica Sinica*, 24(4):1571.
- Jolliffe, I. T. (1982). A note on the use of principal components in regression. *Journal of the Royal Statistical Society: Series C (Applied Statistics)*, 31(3):300–303.
- Lambin, E. F. (1999). Monitoring forest degradation in tropical regions by remote sensing: Some methodological issues. *Global Ecology and Biogeography*, 8(3-4):191–198.
- Maadooliat, M., Huang, J. Z., and Hu, J. (2015). Integrating data transformation in principal components analysis. *Journal of Computational and Graphical Statistics*, 24(1):84–103.
- Panuju, D. R. and Trisasongko, B. H. (2012). Seasonal pattern of vegetative cover from NDVI time-series. *Tropical Forests*, page 255.
- Ramsay, J. O. and Silverman, B. W. (2005). *Functional data analysis*. Springer series in statistics. Springer.
- Shang, H. L. (2013). Functional time series approach for forecasting very short-term electricity demand. *Journal of Applied Statistics*, 40(1):152–168.
- Shang, H. L. (2019). A robust functional time series forecasting method. *Journal of Statistical Computation and Simulation*, 89:795–814.
- Shang, H. L. and Hyndman, R. (2019). *rainbow: Bagplots, Boxplots and Rainbow Plots for Functional Data*. R package version 3.6.0.

- Shen, H. and Huang, J. Z. (2005). Analysis of call centre arrival data using singular value decomposition. *Applied Stochastic Models in Business and Industry*, 21(3):251–263.
- Silverman, B. (1986). *Density estimation for statistics and data analysis*. Chapman & Hall, London.
- Trinka, J., Haghbin, H., and Maadooliat, M. (2020). Multivariate functional singular spectrum analysis over different dimensional domains.
- Tuck, S. L., Phillips, H. R., Hintzen, R. E., Scharlemann, J. P., Purvis, A., and Hudson, L. N. (2014). MODISTools – downloading and processing MODIS remotely sensed data in R. *Ecology and Evolution*, 4(24):4658–4668.
- University of California at Berkely (USA) and Max Planck Institue for Demographic Research (2020). Human mortality database. Data retrieved from <https://www.mortality.org/>.
- Wagner-Muns, I. M., Guardiola, I. G., Samaranyake, V. A., and Kayani, W. I. (2018). A functional data analysis approach to traffic volume forecasting. *IEEE Transactions on Intelligent Transportation Systems*, 19(3):878–888.

Appendix

In this appendix we give a review of the SSA methodology and then we use the results to present the SSA recurrent and vector forecasting algorithms.

SSA Procedure

We consider $\mathbf{y}_N = (y_1, \dots, y_N)^\top \in \mathbb{R}^N$ to be a time series of scalars of length N . Now, we select a lag parameter $1 < L < N/2$, calculate $K = N - L + 1$ and from this we define

$$\mathbf{x}_j := (y_j, \dots, y_{L+j-1})^\top, \quad j = 1, \dots, K$$

to be the j^{th} L -lagged vector. Note that it is common to choose L to be a multiple of the periodicity in the data (Golyandina et al., 2001) and from here we continue on with the SSA algorithm.

Step 1. Embedding

In the embedding step, we form an $L \times K$ trajectory matrix, \mathbf{X} , from the L -lagged vectors where

$$\mathbf{X} = [\mathbf{x}_1, \dots, \mathbf{x}_K].$$

We see that \mathbf{X} is a rank $r = \min\{L, K\}$ matrix and we also have that the columns of \mathbf{X} describe time series behavior over subintervals of time. This stage of embedding can be viewed as applying the invertible transformation $\mathcal{T} : \mathbb{R}^N \rightarrow \mathbb{R}^{L \times K}$ such that $\mathcal{T}(\mathbf{y}_N) = \mathbf{X}$.

Step 2. Decomposition

Now that step 1 is complete, we apply a singular value decomposition (SVD) to the matrix \mathbf{X} to obtain

$$\mathbf{X} = \sum_{i=1}^r \sqrt{\lambda_i} \mathbf{u}_i \mathbf{v}_i^\top$$

where $\{\sqrt{\lambda_i}\}_{i=1}^r$ are singular values, $\{\mathbf{u}_i\}_{i=1}^r$ are left singular vectors, and $\{\mathbf{v}_i\}_{i=1}^r$ are right singular vectors. We call the set $\{\sqrt{\lambda_i}, \mathbf{u}_i, \mathbf{v}_i\}$ as the i^{th} eigentriple of \mathbf{X} and we define $\mathbf{X}_i = \sqrt{\lambda_i} \mathbf{u}_i \mathbf{v}_i^\top$ as the i^{th} , $L \times K$ elementary matrix. From here we go to into the grouping stage.

Step 3. Grouping

For grouping, we partition the set of indices, $\{1, 2, \dots, r\}$, into m disjoint subsets $\{I_1, I_2, \dots, I_m\}$ for $m \leq r$. Now for some positive integer q between 1 and m , we calculate the matrix $\mathbf{X}_{I_q} = \sum_{i \in I_q} \mathbf{X}_i$. From here, we obtain the grouped matrix decomposition

$$\mathbf{X} = \mathbf{X}_{I_1} + \mathbf{X}_{I_2} + \dots + \mathbf{X}_{I_m}.$$

Each \mathbf{X}_{I_q} should correspond to a component in time series decomposition such as trend, seasonal, or noise components, etc.

Step 4. Reconstruction

Our goal now is to reconstruct a FTS that can be used for SSA recurrent forecasting and a matrix that can be used for SSA vector forecasting. First, we transform each \mathbf{X}_{I_q} back into the form of the original series \mathbf{y}_N by the inverse operator \mathcal{T}^{-1} . We achieve

this by first projecting each \mathbf{X}_{I_q} onto $\mathbb{R}_H^{L \times K}$ via orthogonal projection with respect to the Frobenius norm of a matrix where $\mathbb{R}_H^{L \times K}$ is the space of all Hankel $L \times K$ real-valued matrices. We denote this orthogonal projection by $\Pi_H : \mathbb{R}^{L \times K} \rightarrow \mathbb{R}_H^{L \times K}$ and we find that the projection, Π_H , is performed by averaging of the matrix elements over the antidiagonals (where $i + j = \text{const}$). From here, we find that q^{th} additive time series of length N is calculated by $\tilde{\mathbf{y}}_N^q = \mathcal{T}^{-1} \Pi_H(\mathbf{X}_{I_q})$, for $q = 1, \dots, m$. We now let $J \subseteq \{1, \dots, m\}$, then we express a reconstruction as

$$\tilde{\mathbf{y}}_N = \sum_{q \in J} \tilde{\mathbf{y}}_N^q = (\tilde{y}_1, \dots, \tilde{y}_N)^\top.$$

In addition, we also obtain the matrix

$$\mathbf{X}_J = \sum_{q \in J} \mathbf{X}_{I_q} = \left[(\mathbf{x}_J)_1 \cdots (\mathbf{x}_J)_K \right]$$

be used in SSA vector forecasting where $(\mathbf{x}_J)_i \in \mathbb{R}^L$ for $i = 1, \dots, K$.

The reconstruction should be performed in such a way that only the deterministic nature of the original time series, \mathbf{y}_N , is captured in $\tilde{\mathbf{y}}_N$ and \mathbf{X}_J . As a result, often times the number of elements in J is less than m . This allows for $\tilde{\mathbf{y}}_N$ to be governed by a linear recurrent formula so that forecasting of this deterministic signal can be performed (Golyandina et al., 2001). We also call $\mathbf{y}_N - \tilde{\mathbf{y}}_N$ as the residual noisy signal that is not included in our forecasts. From here we move into forecasting of our deterministic signal, $\tilde{\mathbf{y}}_N$.

SSA Recurrent and Vector Forecasting

We first define quantities to be used in the SSA recurrent and vector forecasting algorithms. We denote $\mathbf{x}^\nabla \in \mathbb{R}^{L-1}$ and $\mathbf{x}^\Delta \in \mathbb{R}^{L-1}$ to be the vectors that contain the first and last

(respectively) $L - 1$ components of $\mathbf{x} \in \mathbb{R}^L$. For $k < r$, we define $\mathcal{L} = \text{sp}\{\mathbf{u}_i\}_{i=1}^k$, $\mathcal{L}^\nabla = \text{sp}\{\mathbf{u}_i^\nabla\}_{i=1}^k$, and we define π_i to be the last component from each i^{th} left singular vector for $i = 1, \dots, k$. Next we define $\nu^2 = \sum_{i=1}^k \pi_i^2$ and $\mathbf{g}_{N+M} = (g_1, \dots, g_N, g_{N+1}, \dots, g_{N+M})^\top \in \mathbb{R}^{N+M}$ to be a time series of length $N + M$ and from here, we jump into the SSA-based prediction algorithms.

Recurrent Forecasting

The idea behind the recurrent forecasting algorithm is to express the prediction as a linear combination of the previous $L - 1$ observations of the time series. As according to Golyandina et al. (2001), we first define $\mathbf{h} = (0, \dots, 0, 1)^\top \in \mathbb{R}^L$ and we find that as long as $\mathbf{h} \notin \mathcal{L}$, then

$$g_i = \begin{cases} \tilde{y}_i & i = 1, \dots, N \\ \sum_{j=1}^{L-1} a_j g_{i+j-L} & i = N + 1, \dots, N + M \end{cases} \quad (\text{A1})$$

where the coefficients, $\{a_j\}_{j=1}^{L-1}$, are given in the vector $\mathcal{R} = (a_1, \dots, a_{L-1})^\top = \frac{1}{1-\nu^2} \sum_{n=1}^k \pi_n \mathbf{u}_n^\nabla$. Clearly from the definition of \mathcal{R} , we see what ν^2 must be less than one which implies that $\frac{1}{1-\nu^2} = (1 - \nu^2)^{-1}$ has a geometric series expansion.

Vector Forecasting

The recurrent method has been extended to the vector forecasting realm allowing us to predict observations using L -lagged vectors. We define $\mathbf{U}^\nabla = [\mathbf{u}_1^\nabla \dots \mathbf{u}_k^\nabla] \in \mathbb{R}^{(L-1) \times k}$ and from here, we define the least squares orthogonal projection onto \mathcal{L}^∇ as

$$\Pi = \mathbf{U}^\nabla \left((\mathbf{U}^\nabla)^\top \mathbf{U}^\nabla \right)^{-1} (\mathbf{U}^\nabla)^\top.$$

Now we assume that $\mathbf{h} \notin \mathcal{L}$ and we define the matrix $\mathbf{V} \in \mathbb{R}^{L \times L}$ such that for some $\mathbf{x} \in \mathbb{R}^L$, we have

$$\mathbf{V}\mathbf{x} = \begin{bmatrix} \Pi\mathbf{x}^\Delta \\ \mathcal{R}^\top \Pi\mathbf{x}^\Delta \end{bmatrix} = \begin{bmatrix} \Pi\mathbf{x}^\Delta \\ \mathcal{R}^\top \mathbf{x}^\Delta \end{bmatrix}.$$

Now we define the $L \times (K + M)$ matrix, $Z_J = \left[(\mathbf{z}_J)_1, \dots, (\mathbf{z}_J)_{K+M} \right]$, where

$$(\mathbf{z}_J)_i = \begin{cases} (\mathbf{x}_J)_i & i = 1, \dots, K \\ \mathbf{V}(\mathbf{z}_J)_{i-1} & i = K + 1, \dots, K + M \end{cases}. \quad (\text{A2})$$

From here, we perform antidiagonal averaging on Z_J and we extract \mathbf{g}_{N+M} from the resulting Hankel matrix.

Supplementary Materials

The following contains supplementary materials to the manuscript in order to provide further clarification. We first offer all proofs of theory presented in the manuscript. Next, we give a visuanimation which shows a subset of simulation setups leveraged in the simulation study of the manuscript for futher visualization. Then we give a review of the competing Hyndman and Ullah (2007) method. Then we offer also contains FSSA analysis performed on call center and NDVI data to futher illustrate the existence or lack of periodic or trend behaviors in these datasets.

Proofs

Proof of Thm. 2.1

Fix $\mathbf{e}_x = (0, \dots, 0, x)$ to be a point in \mathcal{H} . Since $\{\boldsymbol{\psi}_j\}_{j=1}^k$ is an orthonormal basis that linearly spans \mathcal{L} , we have that

$$\mathbf{p} = \sum_{j=1}^k \langle \mathbf{e}_x, \boldsymbol{\psi}_j \rangle_{\mathbb{H}^L} \boldsymbol{\psi}_j$$

is the orthogonal projection of \mathbf{e}_x onto \mathcal{L} . Notice that $\langle \mathbf{e}_x, \boldsymbol{\psi}_j \rangle_{\mathbb{H}^L} = \langle x, \pi_j \rangle_{\mathbb{H}}$ for $j = 1, \dots, k$, as such we find that

$$\mathbf{p} = \begin{pmatrix} \sum_{j=1}^k \langle x, \pi_j \rangle_{\mathbb{H}} \psi_{1,j} \\ \vdots \\ \sum_{j=1}^k \langle x, \pi_j \rangle_{\mathbb{H}} \psi_{L-1,j} \\ \sum_{j=1}^k \langle x, \pi_j \rangle_{\mathbb{H}} \pi_j \end{pmatrix} = \begin{pmatrix} \sum_{j=1}^k \langle x, \pi_j \rangle_{\mathbb{H}} \psi_{1,j} \\ \vdots \\ \sum_{j=1}^k \langle x, \pi_j \rangle_{\mathbb{H}} \psi_{L-1,j} \\ \boldsymbol{\nu}(x) \end{pmatrix}.$$

We let $p_{i,j} = \sum_{j=1}^k \langle x, \psi_{i,j} \rangle_{\mathbb{H}}$ for $i = 1, \dots, L-1$, and we find that

$$\|\mathbf{p}\|_{\mathbb{H}^L}^2 = \sum_{i=1}^{L-1} \|p_{i,j}\|_{\mathbb{H}}^2 + \|\mathbf{v}(x)\|_{\mathbb{H}}^2.$$

Since \mathbf{p} is an orthogonal projection of \mathbf{e}_x onto \mathcal{L} , and the projection is non-zero, then, we have that $\|\mathbf{p}\|_{\mathbb{H}^L}^2 = \sum_{i=1}^{L-1} \|p_{i,j}\|_{\mathbb{H}}^2 + \|\mathbf{v}(x)\|_{\mathbb{H}}^2 \leq \|\mathbf{e}_x\|_{\mathbb{H}^L}^2$. This implies that

$$\|\mathbf{v}(x)\|_{\mathbb{H}}^2 \leq \|\mathbf{e}_x\|_{\mathbb{H}^L}^2 = \|x\|_{\mathbb{H}}^2.$$

Since $\|\mathbf{v}(x)\|_{\mathbb{H}}^2 \leq \|x\|_{\mathbb{H}}^2$, we have that \mathbf{v} is in fact a contraction and $\|\mathbf{v}\| < 1$. \square

Proof of Thm. 2.2

Recall that $\{\psi_n^\nabla\}_{n=1}^k$ spans \mathcal{L}^∇ , then for each $\mathbf{v} \in \mathcal{L}^\nabla$ there exists a unique collection of coefficients $\{h_n\}_{n=1}^k$ such that

$$\mathbf{v} = \sum_{n=1}^k h_n \psi_n^\nabla.$$

Also recall that $\{\psi_n\}_{n=1}^k$ spans \mathcal{L} and as such, any $\mathbf{y} \in \mathcal{L}$ can be expressed as

$$\mathbf{y} = \sum_{n=1}^k h_n \psi_n.$$

From this, we see that $\mathbf{y}^\nabla = \sum_{n=1}^k h_n \psi_n^\nabla = \mathbf{v}$. As for the uniqueness of \mathbf{y} , let $\mathbf{y}_1, \mathbf{y}_2 \in \mathcal{L}$ and let $\mathbf{y}_1^\nabla = \mathbf{y}_2^\nabla = \mathbf{v}$, then $\mathbf{y}_1 - \mathbf{y}_2 \in \mathcal{L}$ and is proportional to \mathbf{e}_x which is a contradiction and implies that $\mathbf{y}_1 = \mathbf{y}_2$. Thus, we see that \mathbf{y} must be unique.

Now we show that for some functional L -lagged vector $\mathbf{y} = (y_1, \dots, y_L)^\top \in \mathcal{L}$, the last component $y = y_L$ is a linear combination of the previous $L - 1$ components. Let $\mathbf{v} = (y_1, \dots, y_{L-1})^\top \in \mathcal{L}^\nabla$ and notice that

$$(y_1, \dots, y_{L-1}, \underline{0})^\top + (\underline{0}, \dots, \underline{0}, y)^\top = \sum_{n=1}^k h_n \boldsymbol{\psi}_n. \quad (\text{S1})$$

Taking the inner product of the left and right-hand sides of (S1) with each $\boldsymbol{\psi}_n$ gives us

$$h_n = \langle \boldsymbol{v}, \boldsymbol{\psi}_n^\nabla \rangle_{\mathbb{H}^{L-1}} + \langle y, \pi_n \rangle_{\mathbb{H}}, \quad n = 1, \dots, k. \quad (\text{S2})$$

Notice that we may express y as

$$y = \sum_{n=1}^k h_n \pi_n \quad (\text{S3})$$

and now we substitute in the right-hand side of (S2) for h_n in (S3) to obtain

$$y = \sum_{n=1}^k \langle \boldsymbol{\psi}_n^\nabla, \boldsymbol{v} \rangle_{\mathbb{H}^{L-1}} \pi_n + \boldsymbol{\mathcal{V}}(y).$$

We subtract $\boldsymbol{\mathcal{V}}(y)$ to the left-hand side of the equation, factor out y and then right multiply by $(\boldsymbol{\mathcal{I}} - \boldsymbol{\mathcal{V}})^{-1}$ to obtain

$$y = \sum_{n=1}^k \langle \boldsymbol{\psi}_n^\nabla, \boldsymbol{v} \rangle_{\mathbb{H}^{L-1}} (\boldsymbol{\mathcal{I}} - \boldsymbol{\mathcal{V}})^{-1} \pi_n.$$

Recall that $\langle \boldsymbol{\psi}_n^\nabla, \boldsymbol{v} \rangle_{\mathbb{H}^{L-1}} = \sum_{j=1}^{L-1} \langle \psi_{j,n}, y_j \rangle_{\mathbb{H}}$ and thus

$$\begin{aligned} y &= \sum_{n=1}^k \sum_{j=1}^{L-1} \langle \psi_{j,n}, y_j \rangle_{\mathbb{H}} (\boldsymbol{\mathcal{I}} - \boldsymbol{\mathcal{V}})^{-1} (\pi_n) = \sum_{j=1}^{L-1} \sum_{n=1}^k \psi_{j,n} \otimes (\boldsymbol{\mathcal{I}} - \boldsymbol{\mathcal{V}})^{-1} (\pi_n) (y_j) \\ &= \sum_{j=1}^{L-1} \boldsymbol{\mathcal{A}}_j (y_j) \end{aligned}$$

which shows that the last component of any functional L -lagged vector in \mathcal{L} is a linear combination of the last $L - 1$ components. Now for some $N \in \mathbb{N}$, we obtain

$$g_{N+i} = \sum_{j=1}^{L-1} \mathcal{A}_j g_{N+j-L+i}, \quad i = 1, \dots, M$$

□

Proof of Thm. 2.3

We start by showing that $\mathbf{\Pi}$ is an orthogonal projection onto \mathcal{L}^∇ . First notice that $((\mathcal{P}^\nabla)^* \mathcal{P}^\nabla)^{-1}$ is an $k \times k$ real-valued matrix. Now let $\mathbf{v} \in \mathbb{H}^{L-1}$ and we find that

$$\begin{aligned} \mathbf{\Pi}(\mathbf{\Pi}(\mathbf{v})) &= \mathcal{P}^\nabla ((\mathcal{P}^\nabla)^* \mathcal{P}^\nabla)^{-1} (\mathcal{P}^\nabla)^* \mathcal{P}^\nabla ((\mathcal{P}^\nabla)^* \mathcal{P}^\nabla)^{-1} (\mathcal{P}^\nabla)^* (\mathbf{v}) \\ &= \mathcal{P}^\nabla ((\mathcal{P}^\nabla)^* \mathcal{P}^\nabla)^{-1} (\mathcal{P}^\nabla)^* (\mathbf{v}) \end{aligned}$$

therefore $\mathbf{\Pi}$ is idempotent and is a projector onto \mathcal{L}^∇ .

Now in order to prove the orthogonality of $\mathbf{\Pi}$, we show that it is self-adjoint. Let $\mathbf{u} \in \mathbb{H}^{L-1}$ and notice that

$$\begin{aligned} \langle \mathbf{\Pi}(\mathbf{v}), \mathbf{u} \rangle_{\mathbb{H}^{L-1}} &= \left\langle \mathcal{P}^\nabla ((\mathcal{P}^\nabla)^* \mathcal{P}^\nabla)^{-1} (\mathcal{P}^\nabla)^* (\mathbf{v}), \mathbf{u} \right\rangle_{\mathbb{H}^{L-1}} \\ &= \left\langle \mathcal{P}^\nabla \begin{bmatrix} \sum_{j=1}^k \langle \pi_1, (\mathcal{I} - \mathcal{V})^{-1}(\pi_j) \rangle_{\mathbb{H}} \langle \mathbf{v}, \boldsymbol{\psi}_j^\nabla \rangle_{\mathbb{H}^{L-1}} \\ \vdots \\ \sum_{j=1}^k \langle \pi_j, (\mathcal{I} - \mathcal{V})^{-1}(\pi_j) \rangle_{\mathbb{H}} \langle \mathbf{v}, \boldsymbol{\psi}_j^\nabla \rangle_{\mathbb{H}^{L-1}} \end{bmatrix}, \mathbf{u} \right\rangle_{\mathbb{H}^{L-1}} \\ &= \sum_{j=1}^k \sum_{i=1}^k \langle \pi_j, (\mathcal{I} - \mathcal{V})^{-1}(\pi_i) \rangle_{\mathbb{H}} \langle \boldsymbol{\psi}_j^\nabla, \mathbf{u} \rangle_{\mathbb{H}^{L-1}} \langle \boldsymbol{\psi}_i^\nabla, \mathbf{v} \rangle_{\mathbb{H}^{L-1}}. \end{aligned}$$

In order to continue with the proof, we now show $\langle \pi_j, (\mathcal{I} - \mathcal{V})^{-1}(\pi_i) \rangle_{\mathbb{H}} = \langle \pi_i, (\mathcal{I} - \mathcal{V})^{-1}(\pi_j) \rangle_{\mathbb{H}}$. Notice that $\mathbf{I}_k = (\mathcal{P}^\nabla)^* \mathcal{P}^\nabla + \mathbf{B}$ where \mathbf{I}_k is the $k \times k$ identity matrix and $\mathbf{B} = [\langle \pi_i, \pi_j \rangle_{\mathbb{H}}]$. To this end, $((\mathcal{P}^\nabla)^* \mathcal{P}^\nabla)^{-1} = (\mathbf{I}_k - \mathbf{B})^{-1}$. We define $\mathbf{C} = [\langle \pi_i, (\mathcal{I} - \mathcal{V})^{-1}(\pi_j) \rangle_{\mathbb{H}}]$ and now multiply $(\mathcal{P}^\nabla)^* \mathcal{P}^\nabla (\mathbf{I}_k + \mathbf{C}) = (\mathbf{I}_k - \mathbf{B})(\mathbf{I}_k + \mathbf{C}) = \mathbf{I}_k + \mathbf{C} - \mathbf{BC} - \mathbf{B}$. Now notice that

$$\begin{aligned}
[\mathbf{C} - \mathbf{BC}]_{i,j} &= \langle \pi_i, (\mathcal{I} - \mathcal{V})^{-1}(\pi_j) \rangle_{\mathbb{H}} - \sum_{n=1}^k \langle \pi_i, \pi_n \rangle_{\mathbb{H}} \langle \pi_n, (\mathcal{I} - \mathcal{V})^{-1}(\pi_j) \rangle_{\mathbb{H}} \\
&= \langle \pi_i, (\mathcal{I} - \mathcal{V})^{-1}(\pi_j) \rangle_{\mathbb{H}} - \left\langle \pi_i, \sum_{n=1}^k \langle (\mathcal{I} - \mathcal{V})^{-1}(\pi_j), \pi_n \rangle_{\mathbb{H}} \pi_n \right\rangle_{\mathbb{H}} \\
&= \langle \pi_i, (\mathcal{I} - \mathcal{V})^{-1}(\pi_j) \rangle_{\mathbb{H}} - \left\langle \pi_i, (\mathcal{I} - \mathcal{V})^{-1} \left(\sum_{n=1}^k \langle \pi_j, \pi_n \rangle_{\mathbb{H}} \pi_n \right) \right\rangle_{\mathbb{H}} \\
&= \langle \pi_i, (\mathcal{I} - \mathcal{V})^{-1}(\pi_j) \rangle_{\mathbb{H}} - \langle \pi_i, (\mathcal{I} - \mathcal{V})^{-1}(\mathcal{V}(\pi_j)) \rangle_{\mathbb{H}} \\
&= \langle \pi_i, (\mathcal{I} - \mathcal{V})^{-1}(\pi_j) - (\mathcal{I} - \mathcal{V})^{-1}(\mathcal{V}(\pi_j)) \rangle_{\mathbb{H}} \\
&= \langle \pi_i, (\mathcal{I} - \mathcal{V})^{-1}(\mathcal{I} - \mathcal{V})(\pi_j) \rangle_{\mathbb{H}} \\
&= \langle \pi_i, \pi_j \rangle_{\mathbb{H}} = \mathbf{B}_{i,j}
\end{aligned}$$

and thus, we have $\mathbf{I}_k + \mathbf{C} - \mathbf{BC} - \mathbf{B} = \mathbf{I}_k + \mathbf{B} - \mathbf{B} = \mathbf{I}_k$ which shows that $((\mathcal{P}^\nabla)^* \mathcal{P}^\nabla)^{-1} = (\mathbf{I}_k + \mathbf{C})$. This implies that \mathbf{C} is symmetric and that $\langle \pi_j, (\mathcal{I} - \mathcal{V})^{-1}(\pi_n) \rangle_{\mathbb{H}} = \langle \pi_n, (\mathcal{I} - \mathcal{V})^{-1}(\pi_j) \rangle_{\mathbb{H}}$. This also gives us the form of $((\mathcal{P}^\nabla)^* \mathcal{P}^\nabla)^{-1}$.

Now we continue the proof of $\mathbf{\Pi}$ being self-adjoint by noticing that

$$\begin{aligned}
& \sum_{n=1}^k \sum_{j=1}^k \langle \pi_j, (\mathcal{I} - \mathcal{V})^{-1} (\pi_n) \rangle_{\mathbb{H}} \langle \psi_j^\nabla, \mathbf{u} \rangle_{\mathbb{H}^{L-1}} \langle \psi_n^\nabla, \mathbf{v} \rangle_{\mathbb{H}^{L-1}} \\
&= \sum_{n=1}^k \sum_{j=1}^k \langle \pi_n, (\mathcal{I} - \mathcal{V})^{-1} (\pi_j) \rangle_{\mathbb{H}} \langle \psi_j^\nabla, \mathbf{u} \rangle_{\mathbb{H}^{L-1}} \langle \psi_n^\nabla, \mathbf{v} \rangle_{\mathbb{H}^{L-1}} \\
&= \left\langle \mathbf{v}, \mathcal{P}^\nabla \begin{bmatrix} \sum_{j=1}^k \langle \pi_1, (\mathcal{I} - \mathcal{V})^{-1} (\pi_j) \rangle_{\mathbb{H}} \langle \mathbf{u}, \psi_j^\nabla \rangle_{\mathbb{H}^{L-1}} \\ \vdots \\ \sum_{j=1}^k \langle \pi_k, (\mathcal{I} - \mathcal{V})^{-1} (\pi_j) \rangle_{\mathbb{H}} \langle \mathbf{u}, \psi_j^\nabla \rangle_{\mathbb{H}^{L-1}} \end{bmatrix} \right\rangle_{\mathbb{H}^{L-1}} \\
&= \langle \mathbf{v}, \mathbf{\Pi}(\mathbf{u}) \rangle_{\mathbb{H}^{L-1}}.
\end{aligned}$$

Thus $\mathbf{\Pi}$ is self-adjoint and an orthogonal projection onto \mathcal{L}^∇ .

To finish the proof, we show that $\sum_{j=1}^{L-1} \mathcal{A}_j(\mathbf{\Pi}(\mathbf{y}^\Delta))_j = \sum_{j=1}^{L-1} \mathcal{A}_j(\mathbf{y}^\Delta)_j$ where $\mathbf{y}^\Delta \in \mathbb{H}^{L-1}$. Notice that

$$\sum_{j=1}^{L-1} \mathcal{A}_j(\mathbf{\Pi}(\mathbf{y}^\Delta))_j = \sum_{j=1}^{L-1} \mathcal{A}_j \left(\mathcal{P}^\nabla (\mathbf{I}_k + \mathbf{C}) \begin{bmatrix} \langle \mathbf{y}^\Delta, \psi_1^\nabla \rangle_{\mathbb{H}^{L-1}} \\ \vdots \\ \langle \mathbf{y}^\Delta, \psi_k^\nabla \rangle_{\mathbb{H}^{L-1}} \end{bmatrix} \right)_i = u + v$$

where

$$\begin{aligned}
u &= \sum_{j=1}^{L-1} \mathcal{A}_j \left(\sum_{n=1}^k \langle \mathbf{y}^\Delta, \psi_n^\nabla \rangle_{\mathbb{H}^{L-1}} \psi_{j,n} \right) \\
v &= \sum_{j=1}^{L-1} \mathcal{A}_j \left(\mathcal{P}^\nabla \begin{bmatrix} \sum_{n=1}^k \langle \pi_1, (\mathcal{I} - \mathcal{V})^{-1} (\pi_n) \rangle_{\mathbb{H}} \langle \mathbf{y}^\Delta, \psi_n^\nabla \rangle_{\mathbb{H}^{L-1}} \\ \vdots \\ \sum_{n=1}^k \langle \pi_k, (\mathcal{I} - \mathcal{V})^{-1} (\pi_n) \rangle_{\mathbb{H}} \langle \mathbf{y}^\Delta, \psi_n^\nabla \rangle_{\mathbb{H}^{L-1}} \end{bmatrix} \right)_j.
\end{aligned}$$

Now notice that

$$\begin{aligned}
u &= \sum_{j=1}^{L-1} \sum_{n=1}^k \psi_{j,n} \otimes (\mathcal{I} - \mathcal{V})^{-1} (\pi_n) \left(\sum_{i=1}^r \langle \mathbf{y}^\Delta, \boldsymbol{\psi}_i^\nabla \rangle_{\mathbb{H}^{L-1}} \psi_{j,i} \right) \\
&= \sum_{n=1}^k \sum_{i=1}^d \langle \mathbf{y}^\Delta, \boldsymbol{\psi}_i^\nabla \rangle_{\mathbb{H}^{L-1}} \langle \boldsymbol{\psi}_i^\nabla, \boldsymbol{\psi}_n^\nabla \rangle_{\mathbb{H}^{L-1}} (\mathcal{I} - \mathcal{V})^{-1} (\pi_n) \\
&= \sum_{n=1}^k \sum_{i=1}^k \langle \mathbf{y}^\Delta, \boldsymbol{\psi}_i^\nabla \rangle_{\mathbb{H}^{L-1}} (\mathbf{I}_{i,n} - \langle \pi_i, \pi_n \rangle_{\mathbb{H}}) (\mathcal{I} - \mathcal{V})^{-1} (\pi_n) \\
&= \sum_{n=1}^k \langle \mathbf{y}^\Delta, \boldsymbol{\psi}_n^\nabla \rangle_{\mathbb{H}^{L-1}} (\mathcal{I} - \mathcal{V})^{-1} (\pi_n) - \sum_{i=1}^k \sum_{l_1=1}^{L-1} \langle y_{l_1}^\Delta, \psi_{l_1,i} \rangle_{\mathbb{H}} (\mathcal{I} - \mathcal{V})^{-1} \mathcal{V} (\pi_i) \\
&= \sum_{l_2=1}^{L-1} \mathcal{A}_{l_2} (\mathbf{y}^\Delta)_{l_2} - \mathcal{V} \left(\sum_{l_1=1}^{L-1} \mathcal{A}_{l_1} (\mathbf{y}^\Delta)_{l_1} \right).
\end{aligned}$$

In addition, notice that

$$\begin{aligned}
v &= \sum_{j=1}^{L-1} \mathcal{A}_j \left(\sum_{n_1=1}^k \sum_{n_2=1}^k \langle \pi_{n_1}, (\mathcal{I} - \mathcal{V})^{-1} (\pi_{n_2}) \rangle_{\mathbb{H}} \langle \mathbf{y}^\Delta, \boldsymbol{\psi}_{n_2}^\nabla \rangle_{\mathbb{H}^{L-1}} \boldsymbol{\psi}_{n_1}^\nabla \right)_j \\
&= \sum_{n_3=1}^k \sum_{n_1=1}^k \sum_{n_2=1}^k \langle \pi_{n_1}, (\mathcal{I} - \mathcal{V})^{-1} (\pi_{n_2}) \rangle_{\mathbb{H}} \langle \mathbf{y}^\Delta, \boldsymbol{\psi}_{n_2}^\nabla \rangle_{\mathbb{H}^{L-1}} \langle \boldsymbol{\psi}_{n_1}^\nabla, \boldsymbol{\psi}_{n_3}^\nabla \rangle_{\mathbb{H}^{L-1}} (\mathcal{I} - \mathcal{V})^{-1} (\pi_{n_3}) \\
&= \sum_{n_3=1}^k \sum_{n_1=1}^k \sum_{n_2=1}^k \langle \pi_{n_1}, (\mathcal{I} - \mathcal{V})^{-1} (\pi_{n_2}) \rangle_{\mathbb{H}} \langle \mathbf{y}^\Delta, \boldsymbol{\psi}_{n_2}^\nabla \rangle_{\mathbb{H}^{L-1}} (\mathbf{I}_{n_1, n_3} - \langle \pi_{n_1}, \pi_{n_3} \rangle_{\mathbb{H}}) (\mathcal{I} - \mathcal{V})^{-1} (\pi_{n_3}) \\
&= \sum_{n_1=1}^k \sum_{n_2=1}^k \langle \mathbf{y}^\Delta, \boldsymbol{\psi}_{n_2}^\nabla \rangle_{\mathbb{H}^{L-1}} \langle \pi_{n_1}, (\mathcal{I} - \mathcal{V})^{-1} (\pi_{n_2}) \rangle_{\mathbb{H}} ((\mathcal{I} - \mathcal{V})^{-1} (\pi_{n_1}) - (\mathcal{I} - \mathcal{V})^{-1} \mathcal{V} (\pi_{n_1})) \\
&= \sum_{n_1=1}^k \sum_{n_2=1}^k \langle \mathbf{y}^\Delta, \boldsymbol{\psi}_{n_2}^\nabla \rangle_{\mathbb{H}^{L-1}} \langle \pi_{n_1}, (\mathcal{I} - \mathcal{V})^{-1} (\pi_{n_2}) \rangle_{\mathbb{H}} ((\mathcal{I} - \mathcal{V})^{-1} (\mathcal{I} - \mathcal{V}) (\pi_{n_1})) \\
&= \mathcal{V} \left(\sum_{n_2=1}^k \langle \mathbf{y}^\Delta, \boldsymbol{\psi}_{n_2}^\nabla \rangle_{\mathbb{H}^{L-1}} (\mathcal{I} - \mathcal{V})^{-1} (\pi_{n_2}) \right) \\
&= \mathcal{V} \left(\sum_{j=1}^{L-1} \mathcal{A}_j (\mathbf{y}^\Delta)_j \right).
\end{aligned}$$

As a result, we find that

$$q + r = \sum_{j=1}^{L-1} \mathcal{A}_j (\mathbf{y}^\Delta)_j - \mathcal{V} \left(\sum_{j=1}^{L-1} \mathcal{A}_j (\mathbf{y}^\Delta)_j \right) + \mathcal{V} \left(\sum_{j=1}^{L-1} \mathcal{A}_j (\mathbf{y}^\Delta)_j \right) = \sum_{j=1}^{L-1} \mathcal{A}_j (\mathbf{y}^\Delta)_j.$$

Thus we see that $\sum_{j=1}^{L-1} \mathcal{A}_j (\Pi (\mathbf{y}^\Delta))_j = \sum_{j=1}^{L-1} \mathcal{A}_j (\mathbf{y}^\Delta)_j$

□

Proof of Lemma. 3.1

First notice that

$$\langle (\mathcal{I} - \mathcal{V})(\pi_n), \nu_i \rangle_{\mathbb{H}} = \sum_{l=0}^{\infty} \langle \mathcal{V}^l(\pi_n), \nu_i \rangle_{\mathbb{H}}.$$

As such, we use induction to show the desired result of $[\langle \mathcal{V}^l(\pi_n), \nu_i \rangle_{\mathbb{H}}]_{i=1, \dots, d}^{n=1, \dots, k} = (\mathbf{D}\mathbf{D}^\top)^l \mathbf{D}$.

For our base case, let $l = 1$, then

$$\langle \mathcal{V}(\pi_n), \nu_i \rangle_{\mathbb{H}} = \sum_{n_1=1}^k \langle \pi_n, \pi_{n_1} \rangle_{\mathbb{H}} \langle \pi_{n_1}, \nu_i \rangle_{\mathbb{H}} = (\mathbf{D}\mathbf{D}^\top \mathbf{D})_{i,n}.$$

From here, we state our inductive assumption that $[\langle \mathcal{V}^l(\pi_n), \nu_i \rangle_{\mathbb{H}}]_{i=1, \dots, d}^{n=1, \dots, k} = (\mathbf{D}\mathbf{D}^\top)^l \mathbf{D}$.

Now notice that

$$\begin{aligned} \langle \mathcal{V}^{l+1}(\pi_n), \nu_i \rangle_{\mathbb{H}} &= \sum_{n_1=1}^k \cdots \sum_{n_{l+1}=1}^k \langle \pi_n, \pi_{n_{l+1}} \rangle_{\mathbb{H}} \langle \pi_{n_{l+1}}, \pi_{n_l} \rangle_{\mathbb{H}} \cdots \langle \pi_{n_2}, \pi_{n_1} \rangle_{\mathbb{H}} \langle \pi_{n_1}, \nu_i \rangle_{\mathbb{H}} \\ &= \left((\mathbf{D}\mathbf{D}^\top)^{l+1} \mathbf{D} \right)_{i,n} = \left(\mathbf{D}\mathbf{D}^\top (\mathbf{D}\mathbf{D}^\top)^l \mathbf{D} \right)_{i,n} = \langle \mathcal{V}(\mathcal{V}^l(\pi_n)), \nu_i \rangle_{\mathbb{H}}. \end{aligned}$$

which shows the desired result. As such, we see that

$$\langle (\mathcal{I} - \mathcal{V})^{-1}(\pi_n), \nu_i \rangle_{\mathbb{H}} = \sum_{l=0}^{\infty} \langle \mathcal{V}^l(\pi_n), \nu_i \rangle_{\mathbb{H}} = \left(\left(\sum_{l=0}^{\infty} (\mathbf{D}\mathbf{D}^\top)^l \right) \mathbf{D} \right)_{i,n}.$$

□

Proof of Thm. 3.1

As according to Balazs (2009), we find that the matrix $\mathbf{A}_j \in \mathbb{R}^{d \times d}$ has entries

$$(\mathbf{A}_j)_{k_1, k_2} = \langle \mathcal{A}_j(\nu_{k_2}), \nu_{k_1} \rangle_{\mathbb{H}} = \sum_{n=1}^k \langle \nu_{k_2}, \psi_{j,n} \rangle_{\mathbb{H}} \langle (\mathcal{I} - \mathcal{V})^{-1}(\pi_n), \nu_{k_1} \rangle_{\mathbb{H}}.$$

We use the result of Lemma 3.1 and obtain

$$(\mathbf{A}_j)_{k_1, k_2} = \left(\sum_{l=0}^{\infty} (\mathbf{D}\mathbf{D}^\top)^l \right) \mathbf{D}\mathbf{E}_j^\top.$$

□

Proof of Thm. 3.2 As according to Balazs (2009), we find that the matrix $\mathbf{P} \in \mathbb{R}^{(L-1)d \times (L-1)d}$ has entries of the form

$$(\mathbf{P})_{i,j} = \langle \Pi(\phi_j^\nabla), \phi_i^\nabla \rangle_{\mathbb{H}^{(L-1)d}}.$$

We now see that

$$\begin{aligned} \langle \Pi(\phi_j^\nabla), \phi_i^\nabla \rangle_{\mathbb{H}^{L-1}} &= \left\langle \mathcal{P}^\nabla \left((\mathbf{I}_k + \mathbf{C}) \begin{bmatrix} \langle \phi_j^\nabla, \psi_1^\nabla \rangle_{\mathbb{H}^{L-1}} \\ \vdots \\ \langle \phi_j^\nabla, \psi_k^\nabla \rangle_{\mathbb{H}^{L-1}} \end{bmatrix} \right), \phi_i^\nabla \right\rangle_{\mathbb{H}^{L-1}} \\ &= \left\langle \mathcal{P}^\nabla \left(\begin{bmatrix} \langle \phi_j^\nabla, \psi_1^\nabla \rangle_{\mathbb{H}^{L-1}} \\ \vdots \\ \langle \phi_j^\nabla, \psi_r^\nabla \rangle_{\mathbb{H}^{L-1}} \end{bmatrix} \right) + \mathcal{P}^\nabla \left(\begin{bmatrix} \sum_{n=1}^k \langle \pi_1, (\mathcal{I} - \mathcal{V})^{-1}(\pi_n) \rangle_{\mathbb{H}^{L-1}} \langle \phi_j^\nabla, \psi_n^\nabla \rangle_{\mathbb{H}^{L-1}} \\ \vdots \\ \sum_{n=1}^k \langle \pi_k, (\mathcal{I} - \mathcal{V})^{-1}(\pi_n) \rangle_{\mathbb{H}^{L-1}} \langle \phi_j^\nabla, \psi_n^\nabla \rangle_{\mathbb{H}^{L-1}} \end{bmatrix} \right), \phi_i^\nabla \right\rangle_{\mathbb{H}^{L-1}} \\ &= \sum_{l=1}^k \langle \phi_j^\nabla, \psi_l^\nabla \rangle_{\mathbb{H}^{L-1}} \langle \psi_l^\nabla, \phi_i^\nabla \rangle_{\mathbb{H}^{L-1}} + \sum_{l=1}^r \sum_{n=1}^k \langle \phi_i^\nabla, \psi_l^\nabla \rangle_{\mathbb{H}^{L-1}} \langle \pi_l, (\mathcal{I} - \mathcal{V})^{-1}(\pi_n) \rangle_{\mathbb{H}^{L-1}} \langle \psi_n^\nabla, \phi_j^\nabla \rangle_{\mathbb{H}^{L-1}} \\ &= \left(\mathbf{F}\mathbf{F}^\top + \mathbf{F}\mathbf{D}^\top \sum_{l=0}^{\infty} (\mathbf{D}\mathbf{D}^\top)^l \mathbf{D}\mathbf{F}^\top \right)_{i,j=1}^{(L-1)d} \end{aligned}$$

□

Simulated Data

In order to further clarify what varying simulation setups from the manuscript look like, we consider a subset of the different cases where we change the periodicity in the data, the trend, and the noise structure. We hold $L = 40$, $N = 200$, and $M = 80$ constant and we generate the visuanimation of Figure S1 which shows the testing set true signal we are trying to predict in plot (A), the rolling forecast prediction of the testing set using the method of Hyndman and Ullah (2007) (B), the rolling forecast prediction using V-forecasting in plot (C), and the rolling forecast prediction using R-forecasting in plot (D). The first four frames of the animation are concerned with simulated data where only periodicity is present, the next four are concerned with cases where there is a mix of periodicity and trend, and the last four frames consider setups where there is only trend in the data.

Figure S1: Plot (A): testing set true signal, Plot (B): forecast of testing set using method of Hyndman and Ullah (2007), Plot (C): V-forecast of testing set, Plot (D): R-forecast of testing set. The last four figures in that animation were generated using **rainbow** (Shang and Hyndman, 2019).

For the last four figures in the visuanimation, warmer colors are indicative of observations from earlier time points while cooler colors are indicative of observations of later time points.

Real Data

Here, we give further justification to the claims in the manuscript that there exists a strong weekly periodicity in the call center data with no trend and that there's a mix of periodicity and trend present in the NDVI data. We do not argue the lack of periodicity and presence of trend in the mortality rate data as this can be inferred from plot (C) of Figure 2 of the manuscript. This section is to be viewed as a summary of results in Haghbin et al. (2020a) and all of the following figures are drawn directly from that work and the corresponding supplement of Haghbin et al. (2020b). We begin with analysis of the call center data. To start, we offer Figure S2 which shows a clear weekly pattern is present in the raw data where the function observed, depends on the day of the week.

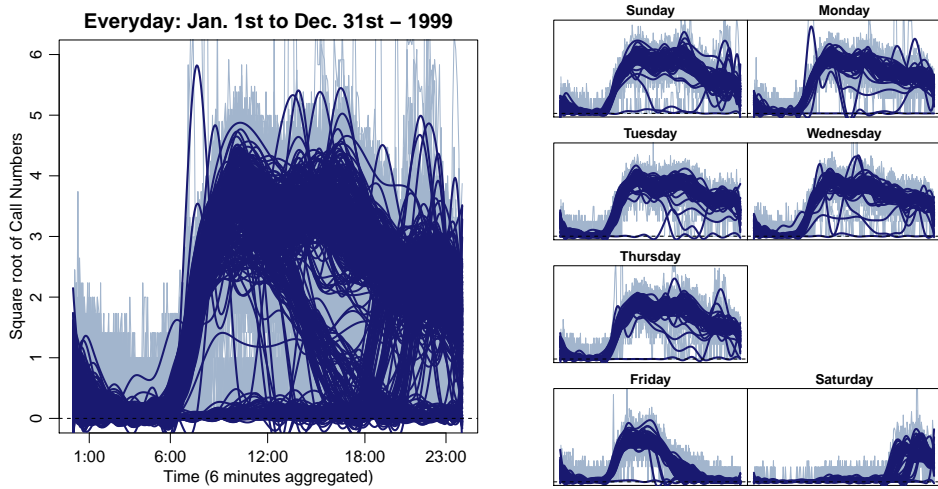


Figure S2: The number of calls to a call center between January 1st to December 31st in the year 1999.

Applying FSSA with a lag of 28 to the call center data, just like in Haghbin et al.

(2020a), gives us the singular values of Figure S3 plot (A), the w -correlation matrix of plot (B), right singular vectors of plot (C), and pair plot of singular vectors (D).

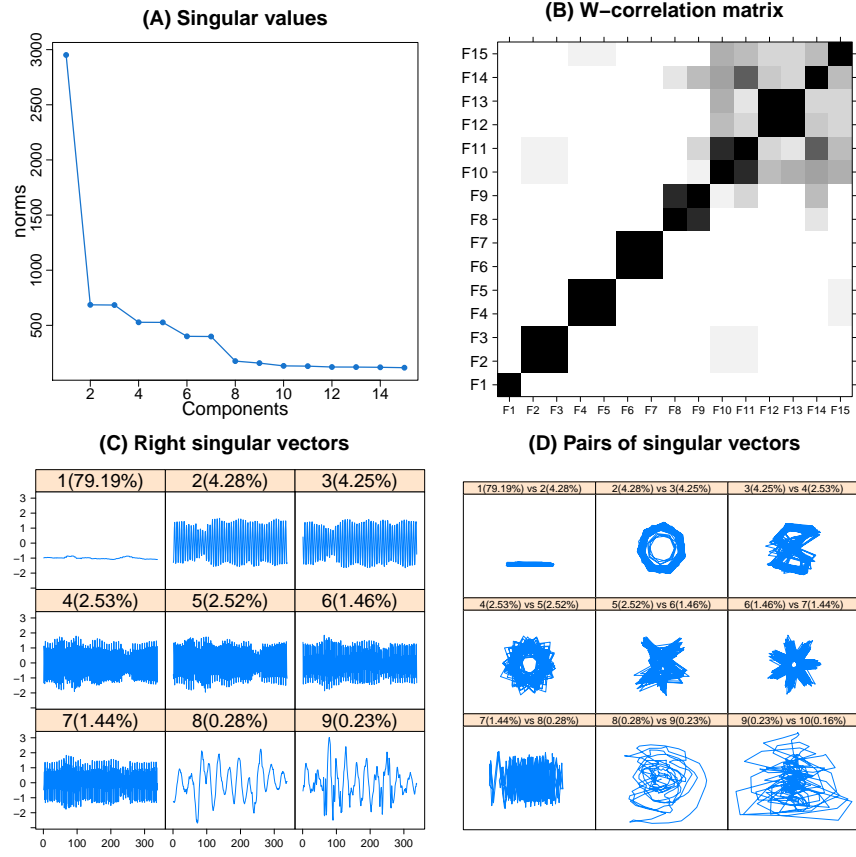


Figure S3: Plot (A): singular values, Plot (B): w -correlation matrix, Plot (C): right singular vectors, Plot (D): pair plots of right singular vectors. For more information on these plots, we refer to Hagbin et al. (2020a).

We see from Figure S3, plots (A) and (B) that there are seven components that do not correspond to noise and plots (C) and (D) show that components two through 7 reflect

weekly periodicity. We see that plot (C) has oscillations in the weights that are multiplied by each left singular function indicating periodicity. Furthermore, the pair plots of 2 vs. 3, 4 vs. 5, and 6 vs. 7 in plot (D) of Figure S3 clearly shows the weekly pattern as according to the 7 sharp corners in each plot. To further argue a seven day weekly pattern, we plot the resulting left singular functions in Figure S4.

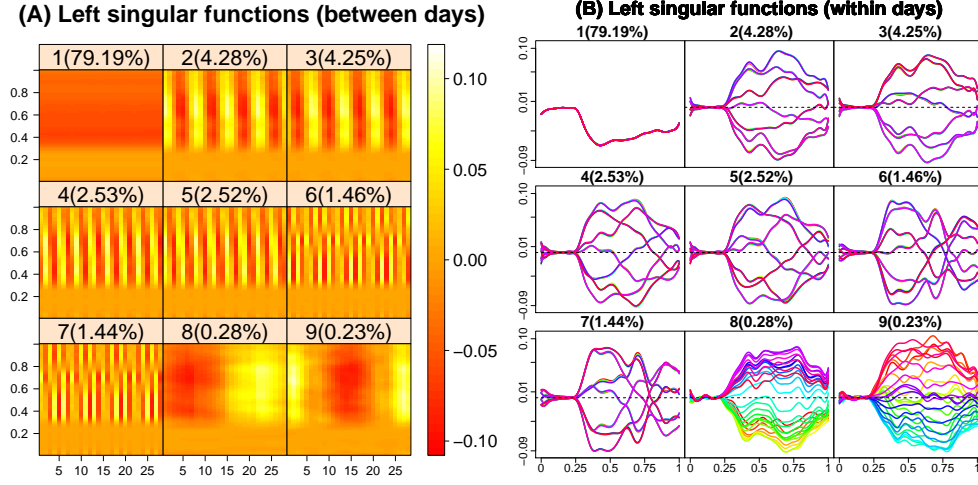


Figure S4: Plot (A): heat map of left singular functions, Plot (B): left singular functions.

Here, we clearly see a weekly periodicity in components two through seven where we find the oscillatory behavior in plot (A) between days and we count seven distinct curves in subplots two through seven of plot (B). From this analysis, we confirm the presence of highly periodic components in the call center data and we also notice that there are no significant trend components to be found.

We now argue the existence of periodic and trend components in the NDVI data. We first give an example of an NDVI image and the corresponding density of NDVI we estimate that are shown in Figure S5.

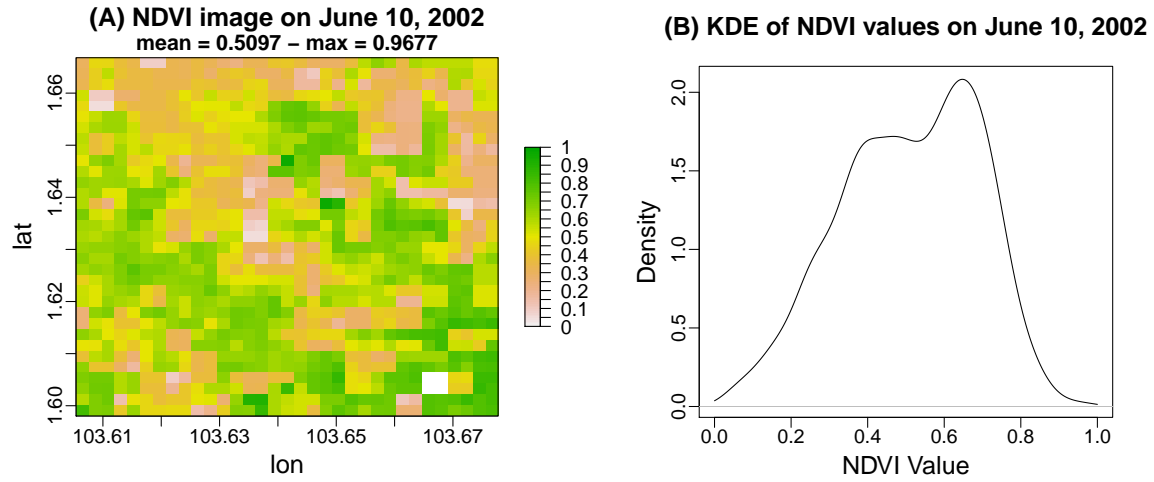


Figure S5: Plot (A): sample NDVI image, Plot (B): the corresponding estimated density of NDVI

Just like in Haghbin et al. (2020a), we apply FSSA to the 448 NDVI densities with a lag of 45 and we obtain the exploratory plots of Figure S6.

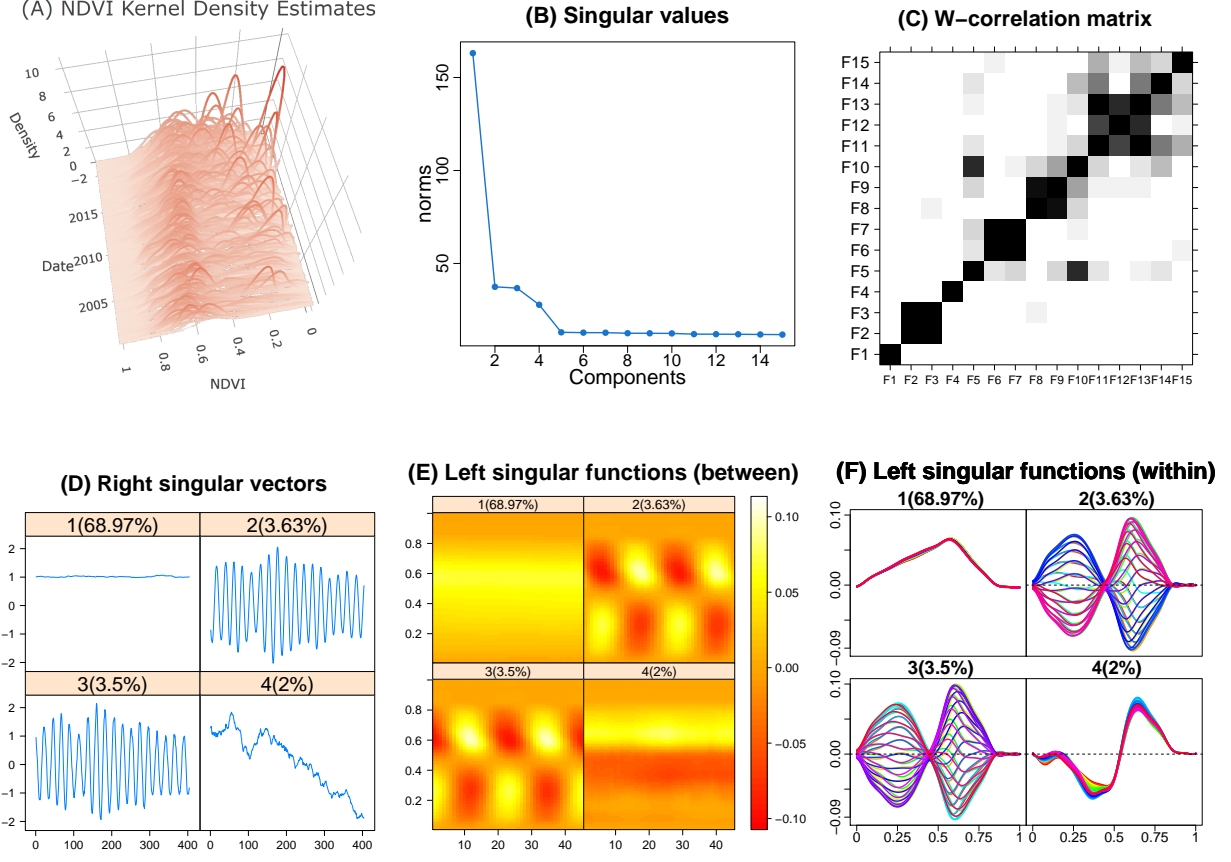


Figure S6: The KDEs of the 448 NDVI images, plus the FSSA plots for the grouping steps of the NDVI dataset.

Plot (A) of Figure S6 shows a 3-D plot of the NDVI densities, (B) and (C) show that there are four components that don't correspond to noise, and plots (D), (E), and (F) show the existence of yearly periodicity in components 2 and 3 while component four captures a trend behavior in the data. We see that component four is a trend because after 2010 (210

on x axis of plot (D)), we switch from weighting the fourth left singular function seen in plot (F), positively, to negatively such that instead of weighting heavily around 0.60, we weight more heavily around NDVI values of 0.4.

Approach of Hyndman and Ullah to FTS Forecasting

The approach Hyndman and Ullah (2007) leverages a weighted FPCA of a FTS to find basis elements that explain variation. They then project their time dependent data onto the basis in order to find scores for each principal component. Finally, they perform forecasting techniques such as ARIMA on the resulting principal component scores in order to predict future observations of the FTS. The following steps outline the process.

1. Smooth the FTS using a nonparametric smoothing method to estimate $f_t(x)$ for $x \in [x_1, x_p]$ from sampling points $\{x_i, y_t(x_i)\}$, $i = 1, \dots, p$ where $f_t(x)$ is a function observed on day t and p is the number of sampling points
2. Decompose the fitted observations using a weighted FPCA to obtain the basis expansion of

$$f_t(x) = \mu(x) + \sum_{k=1}^K \beta_{t,k} \phi_k(x) + e_t(x)$$

where $\mu(x)$ is the mean function, $\{\phi_k(x)\}_{k=1}^K$ is a set of orthonormal basis functions (notice we truncate at K basis elements), $e_t(x) \sim N(0, \nu(x))$, and $\nu(x)$ is the covariance function

3. Fit univariate time series models, such as ARIMA, to each of the coefficients $\{\beta_{t,k}\}_{k=1}^K$

4. Forecast the coefficients $\{\beta_{t,k}\}_{k=1}^K$ for $t = n + 1, \dots, n + h$ using the fitted time series models where n is the length of the FTS and h is the forecast horizon
5. Multiply the forecasted coefficients by their respective k^{th} basis elements to forecast $\{f_{n+1}(x), \dots, f_{n+h}(x)\}$.